2st Advanced Course on Radar Polarimetry

ESA ESRIN, Frascati, 2011

Multi-baseline PolInSAR

Basic concepts and methods

Stefano Tebaldini*

Dipartimento di Elettronica e Informazione

Politecnico di Milano

**with a lot of help from Mauro Mariotti d'Alessandro, Ho Tong Minh Dinh, Fabio Rocca (PoliMi)*

Why multiple baselines?

Multiple baselines ⬄ Illumination from multiple points of view

Multi-baseline (MB) systems:

- Multiple pass systems:

  airborne and spaceborne SARs
- Multiple antenna systems:

  ground based Radars

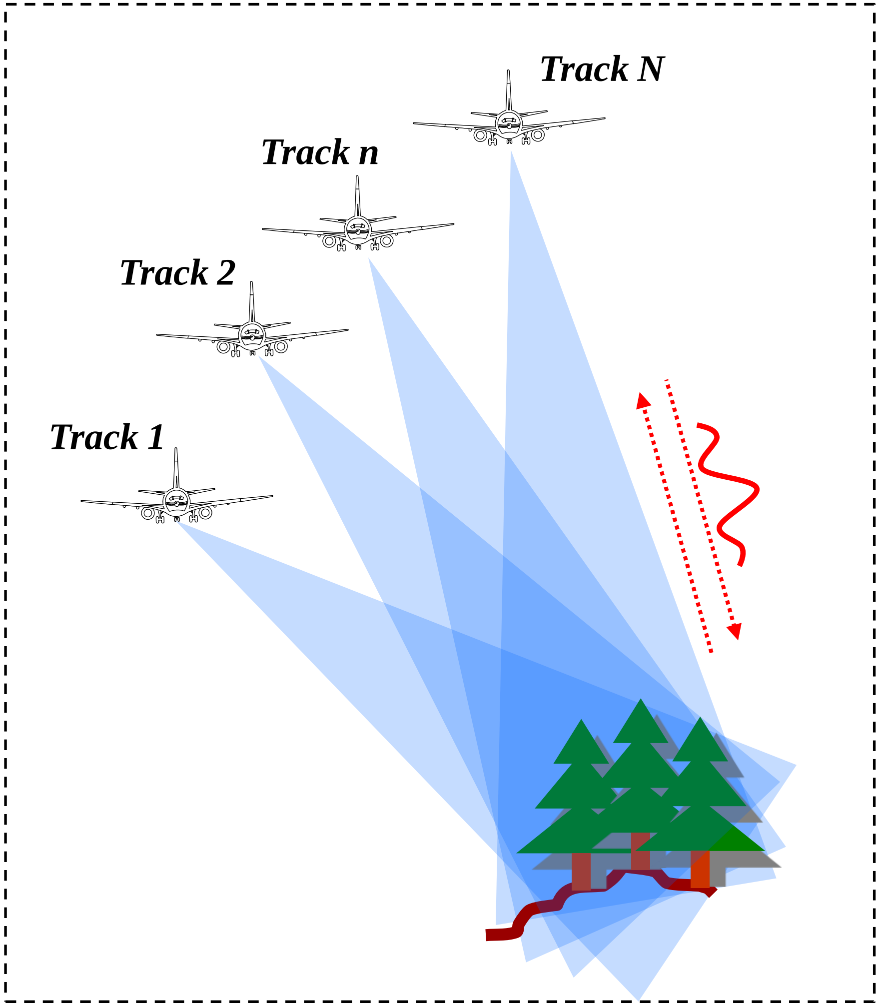

MB campaigns involve:

- Higher costs:

  spaceborne: ≈ *x 1*

  ground based: ≈ *x N*
- More sophisticated processing:

  see single vs multi-baseline InSAR…

MB systems offers one important advantage: more equations

⇒ Increased robustness against disturbances (temporal decorrelation…)

and/or Relaxation of hypotheses required in the single baseline case

MB systems offers one important advantage: more equations

⇒ Increased robustness against disturbances (temporal decorrelation…)

and/or Relaxation of hypotheses required in the single baseline case

⇒ More unknowns are available to characterize the vertical structure of the scene

MB systems offers one important advantage: more equations

⇒ Increased robustness against disturbances (temporal decorrelation…)
and/or Relaxation of hypotheses required in the single baseline case

⇒ More unknowns are available to characterize the vertical structure of the scene

MB allow to pass from model based inversion to full Tomographic reconstruction

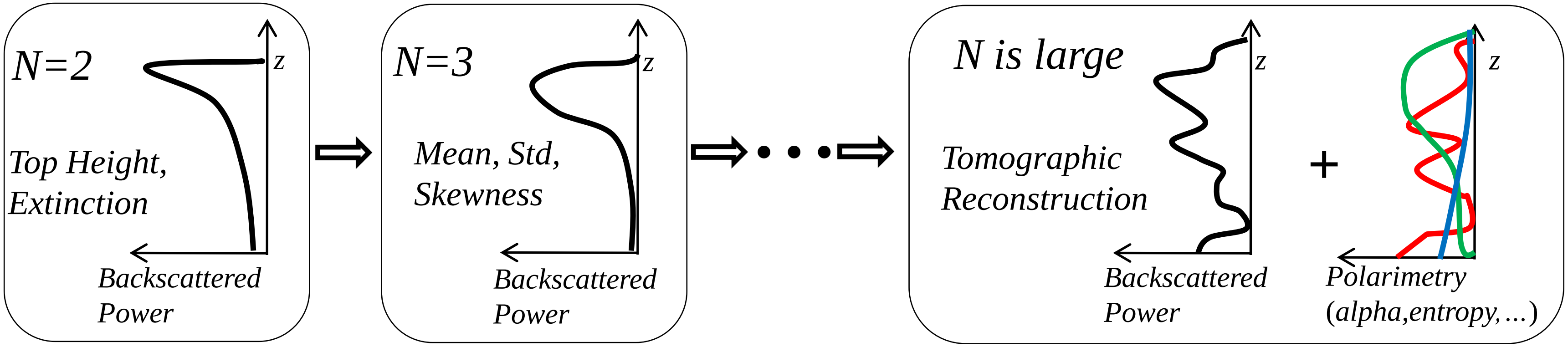

MB PolInSAR provide access to the 3D distribution of the polarimetric properties of the scene

Outline

Introduction to SAR Tomography

- Basic Concepts
- Tomographic Scene Reconstruction
- Polarimetry and Tomography: Examples
- Phase Calibration

Optimization Methods

- Multi-layer Optimization
- Multi-baseline Coherence Optimization

Ground-volume Decomposition

- Problem Statement
- SKP Structure
- SKP Decomposition
- Regions of Physical Validity
- Boundary Solutions
- Case Studies

Conclusions

MB PolInSAR

Vertical resolution ≈ 1 ÷ 15 m
N ≈ 6 ÷ 50

Vertical resolution ≈ 10 ÷ 30 m
N ≈ 6 ÷ 15

Vertical resolution >> 30 m
N ≥ 2

Single Baseline PolInSAR
N = 2

Outline

Introduction to SAR Tomography

- Basic Concepts
- Tomographic Scene Reconstruction
- Polarimetry and Tomography: Examples

Optimization Methods

- Multi-layer Optimization
- Multi-baseline Coherence Optimization

Ground-volume Decomposition

- Problem Statement
- SKP Structure
- SKP Decomposition
- Regions of Physical Validity
- Boundary Solutions
- Case Studies

Conclusions

MB PolInSAR

Vertical resolution ≈ 1 ÷ 15 m
N ≈ 6 ÷ 50

Vertical resolution ≈ 10 ÷ 30 m
N ≈ 6 ÷ 15

Vertical resolution >> 30 m
N ≥ 2

Single Baseline PolInSAR
N = 2

Basic Concepts

Multiple baselines ⇔ Illumination from multiple points of view

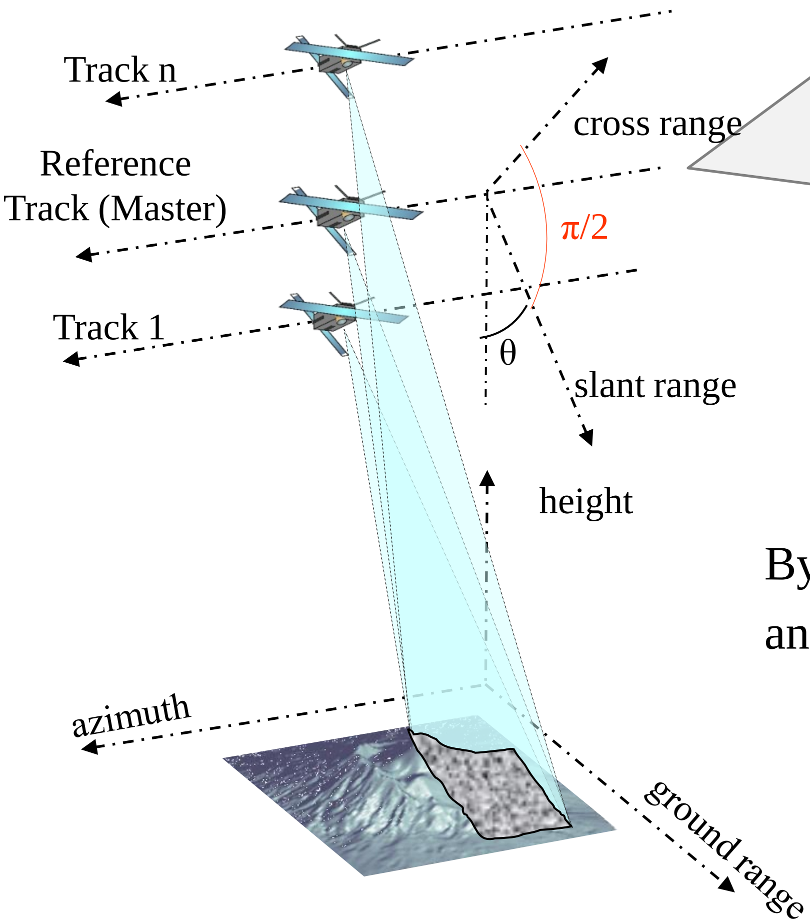

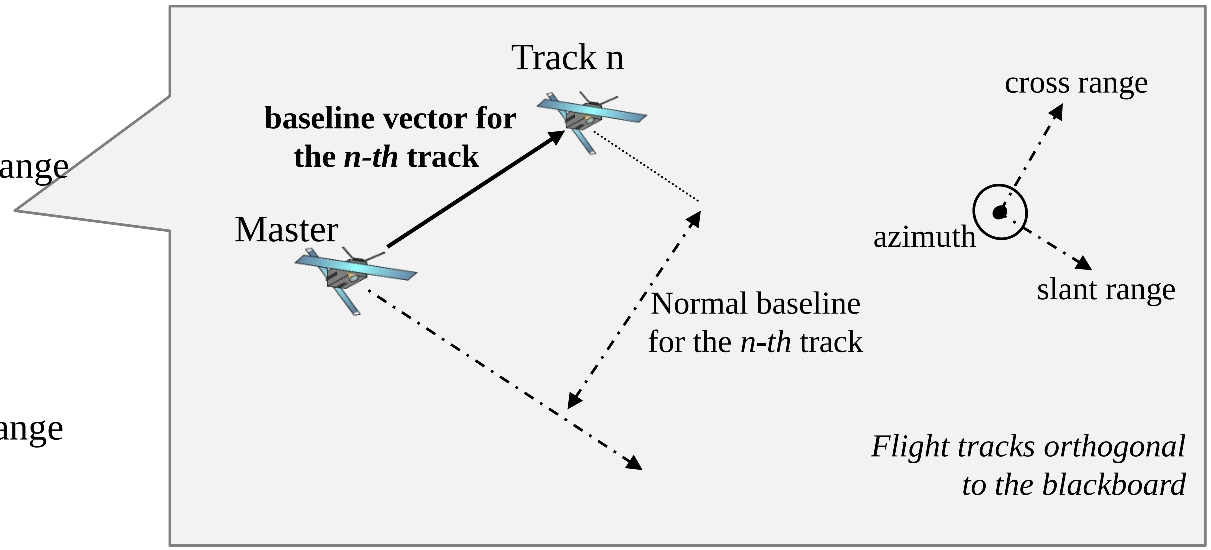

By collecting several baselines it is possible to synthesize an antenna along the cross range direction as well

⇩

3D focusing is possible in the coordinate system: *slant range, azimuth, cross range*

Resolution is determined by pulse bandwidth along the slant range direction, and by the lengths of the synthetic apertures in the azimuth and cross range directions

⇒The SAR resolution cell is split into **multiple layers**, according to baseline aperture

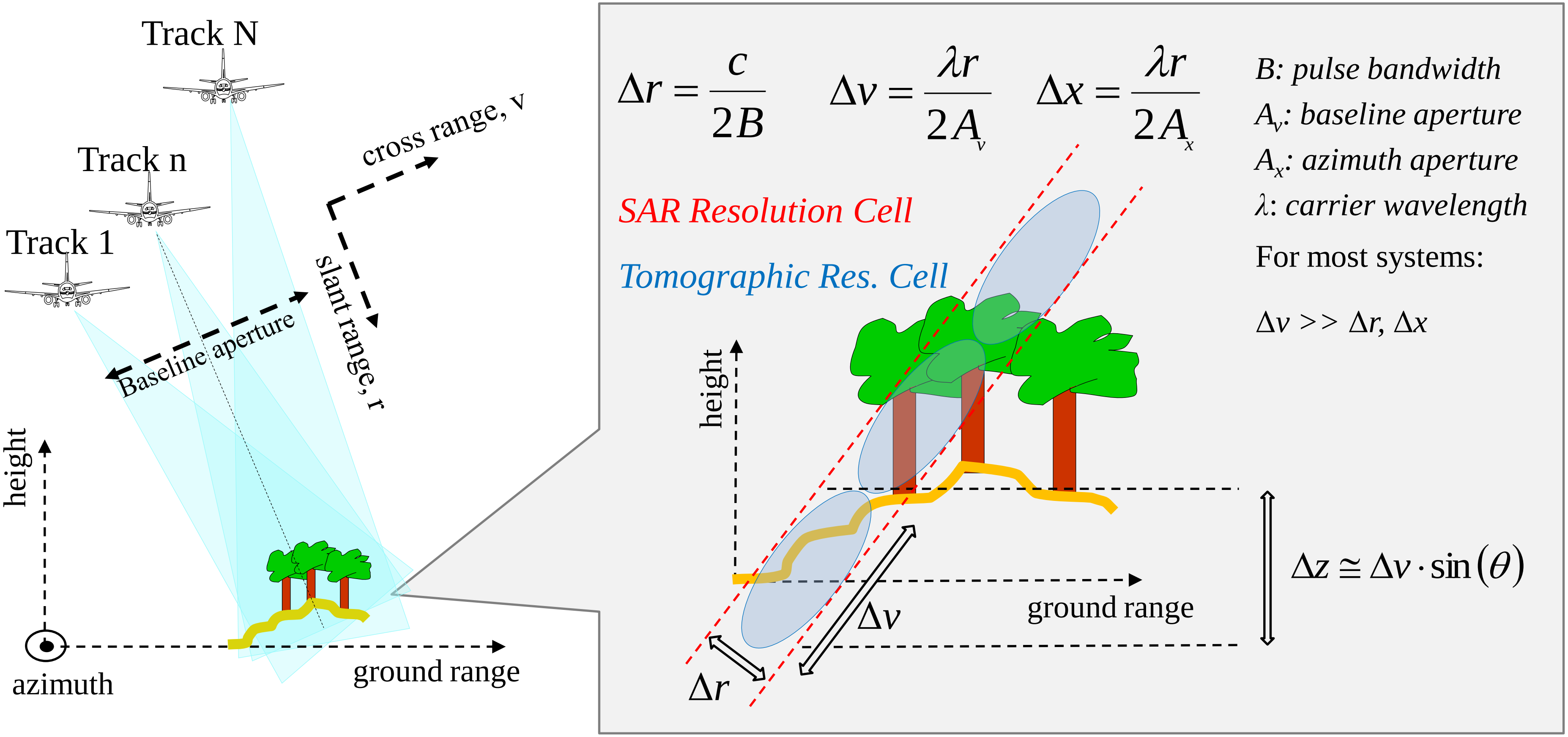

Tomographic Scene Reconstruction

Assuming typical airborne or spaceborne MB geometries, SAR Tomography can be formulated according to one simple principle:

Each focused SLC SAR image is obtained as the Fourier Transform of the scene complex reflectivity along the cross-range coordinate

$$y_n(r,x) = \int s(r,x,v) \exp\left(-j\frac{4\pi}{\lambda r} b_n v\right) dv$$

$y_n(r,x)$: SLC pixel in the *n-th* image

$s(r,x,v)$: average complex reflectivity of the scene within the SAR 2D resolution cell at (r,x)

b_n : normal baseline for the *n-th* image

λ : carrier wavelength

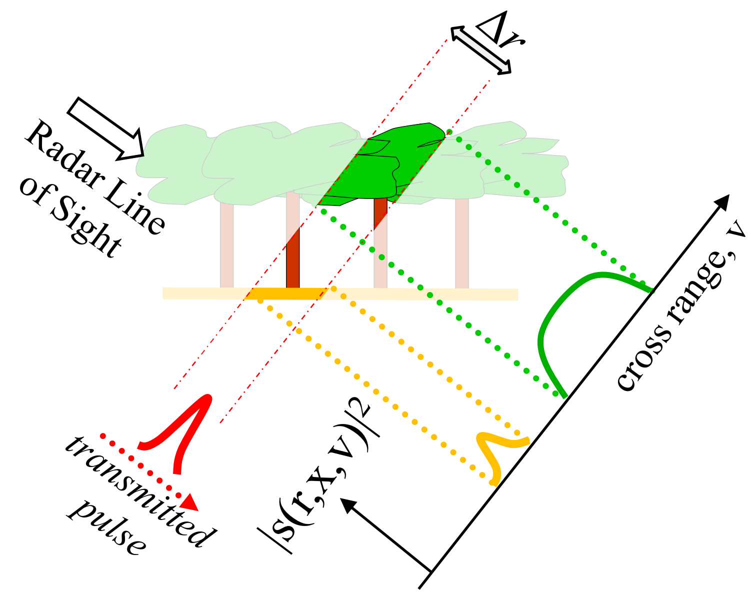

⇒ The cross-range distribution of the complex reflectivity can be retrieved through Fourier-based techniques

Performances are often limited by baseline sparseness and aperture

⇒ SAR Tomography is commonly rephrased as a Spectral Estimation problem, based on the analysis of the data covariance matrix among different tracks

General Procedure

Form the MB data vector [Nx1]

$$\mathbf{y}_{MB} = \begin{bmatrix} y_1(r,x) \\ y_2(r,x) \\ \vdots \\ y_N(r,x) \end{bmatrix}$$

⇒

Evaluate the sample covariance matrix [NxN] by local multi-looking

$$\hat{\mathbf{R}} = \left\langle \mathbf{y}_{MB}\mathbf{y}_{MB}^{H} \right\rangle_L$$

⇒

Evaluate the cross-range distribution of the backscattered power through some Spectral Estimator

$$\left|\hat{s}(r,x,v)\right|^2 = \hat{S}(v)$$

Remark: it is customary to normalize **R** such that entries on the main diagonal are unitary

⇔ **R** is the matrix of the interferometric coherences for all baselines

$$\{\mathbf{R}\}_{nm} = \frac{E\left[y_n y_m^*\right]}{\sqrt{E\left[\left|y_n\right|^2\right]E\left[\left|y_m\right|^2\right]}} = \gamma_{nm}$$

Spectral Estimators :

- Beamforming:

inverse Fourier Transform; coarse spatial resolution; radiometrically consistent

$$\hat{S}(v) = \mathbf{a}^H(v)\hat{\mathbf{R}}\mathbf{a}(v) \qquad \mathbf{a}(v) = \left[\exp\left(j\frac{4\pi}{\lambda r}b_1 v\right) \quad \exp\left(j\frac{4\pi}{\lambda r}b_2 v\right) \quad \cdots \quad \exp\left(j\frac{4\pi}{\lambda r}b_N v\right)\right]^T$$

- Capon Spectral Estimator:

spatial resolution is greatly enhanced, at the expense of radiometric accuracy; $\hat{S}(v) = \dfrac{1}{\mathbf{a}^H(v)\hat{\mathbf{R}}^{-1}\mathbf{a}(v)}$

- Methods based on the analysis of the eigenstructure of **R** (MUSIC, ESPRIT…):

determination of the dominant scatterering centers; mostly suited for urban scenarios

- Methods based on sectorial information (Truncated SVD, PCT…):

optimal basis choice (e.g.: Legendre), depending on a-priori info about the scene vertical extent

- Model based methods (NLS, COMET…):

model based; high radiometric accuracy; high computational burden; possible model mismatches

- Compressive sensing:

localization of few scattering centers via L1 norm minimization; mostly suited for urban scenarios

Example: Tomographic reconstruction of a forest scenario

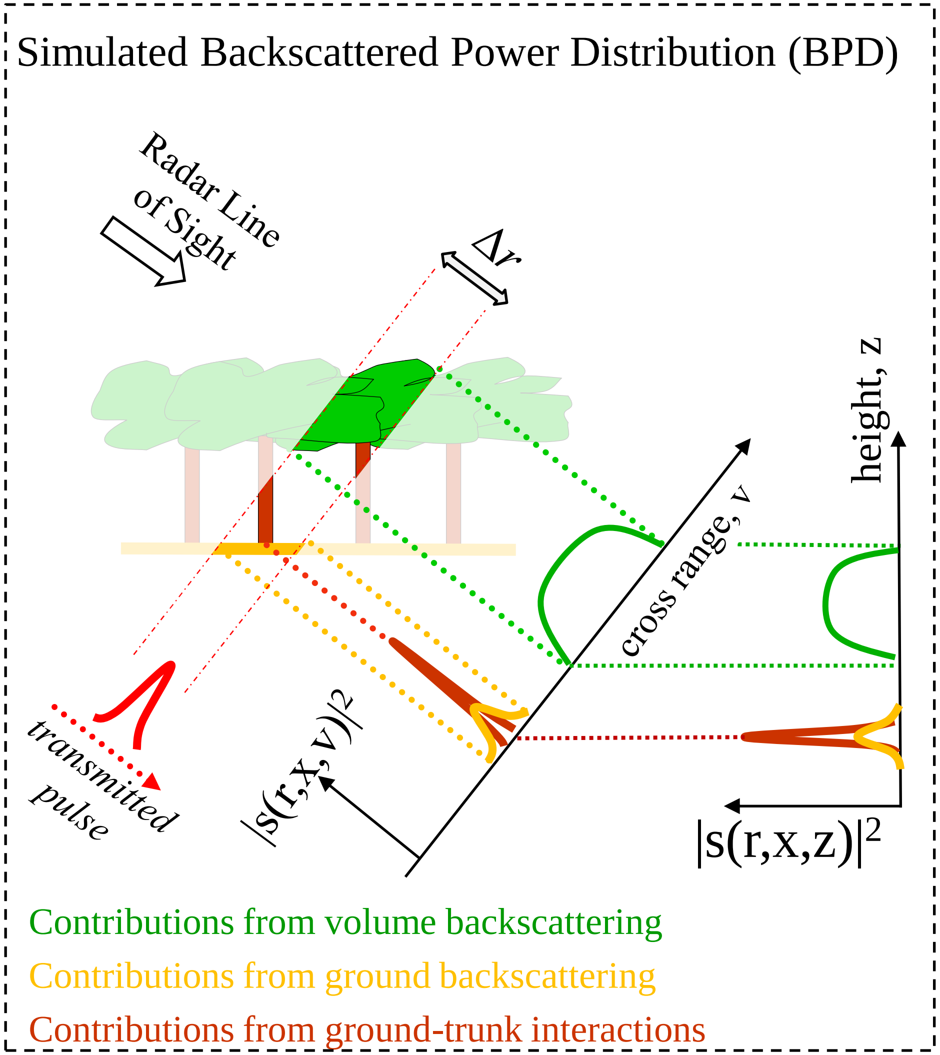

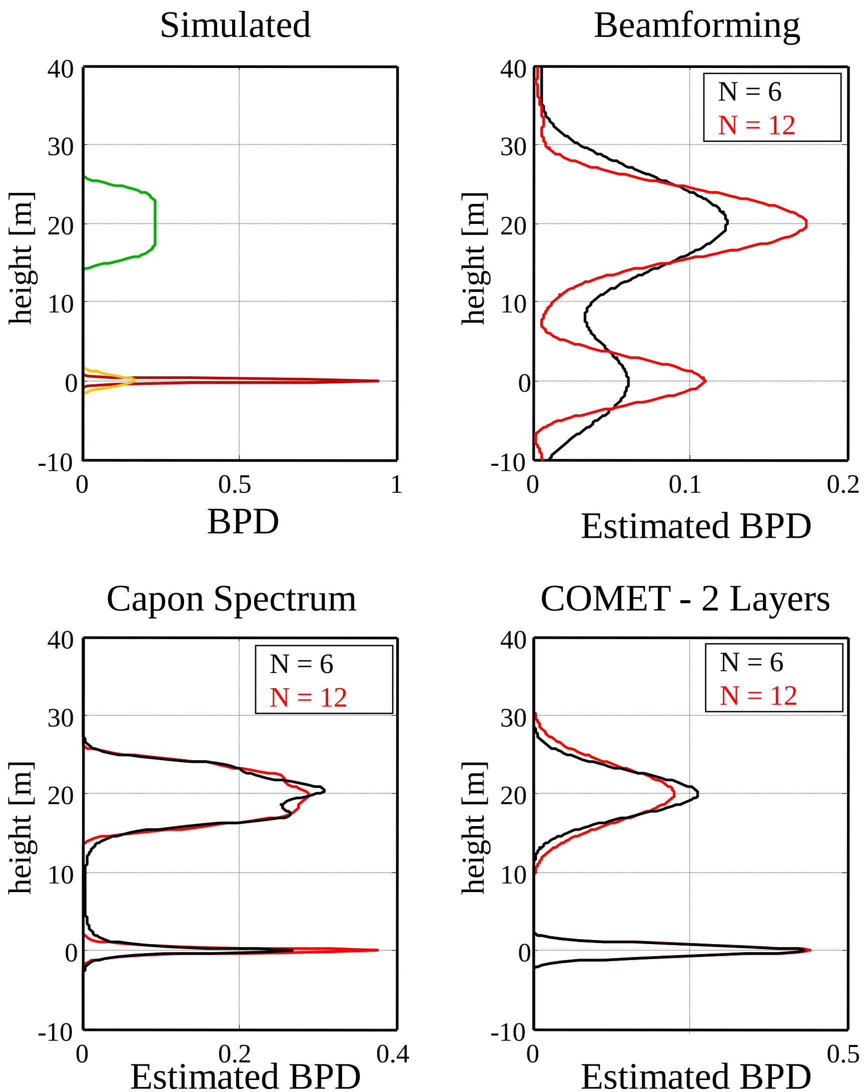

Polarimetry and Tomography: Examples

Campaign	BioSAR 2007 - ESA
System	E-SAR - DLR
Period	Spring 2007
Site	Remningstorp, South Sweden
Scene	Semi-boreal forest
Topography	Flat
Tomographic tracks	9 – Fully Polarimetric
Carrier frequency	350 MHz
Slant range resolution	2 m
Azimuth resolution	1.6 m
Vertical resolution	10 m (near range) to 40 m (far range)

Tomographic reconstruction of an azimuth cut:

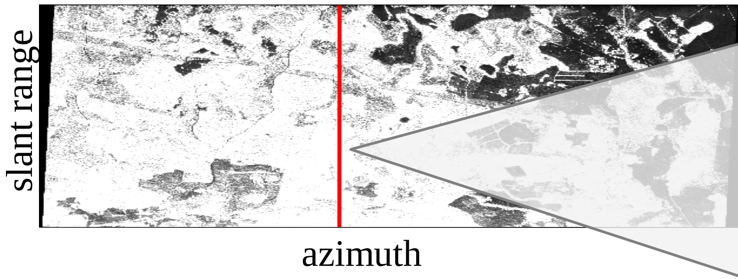

The analyzed profile is almost totally forested, except for the dark areas

HH:
- Dominant phase center is ground locked
- Vegetation is barely visible

Similar conclusions for VV

HV:
- Dominant phase center is ground locked
- Vegetation is much more visible

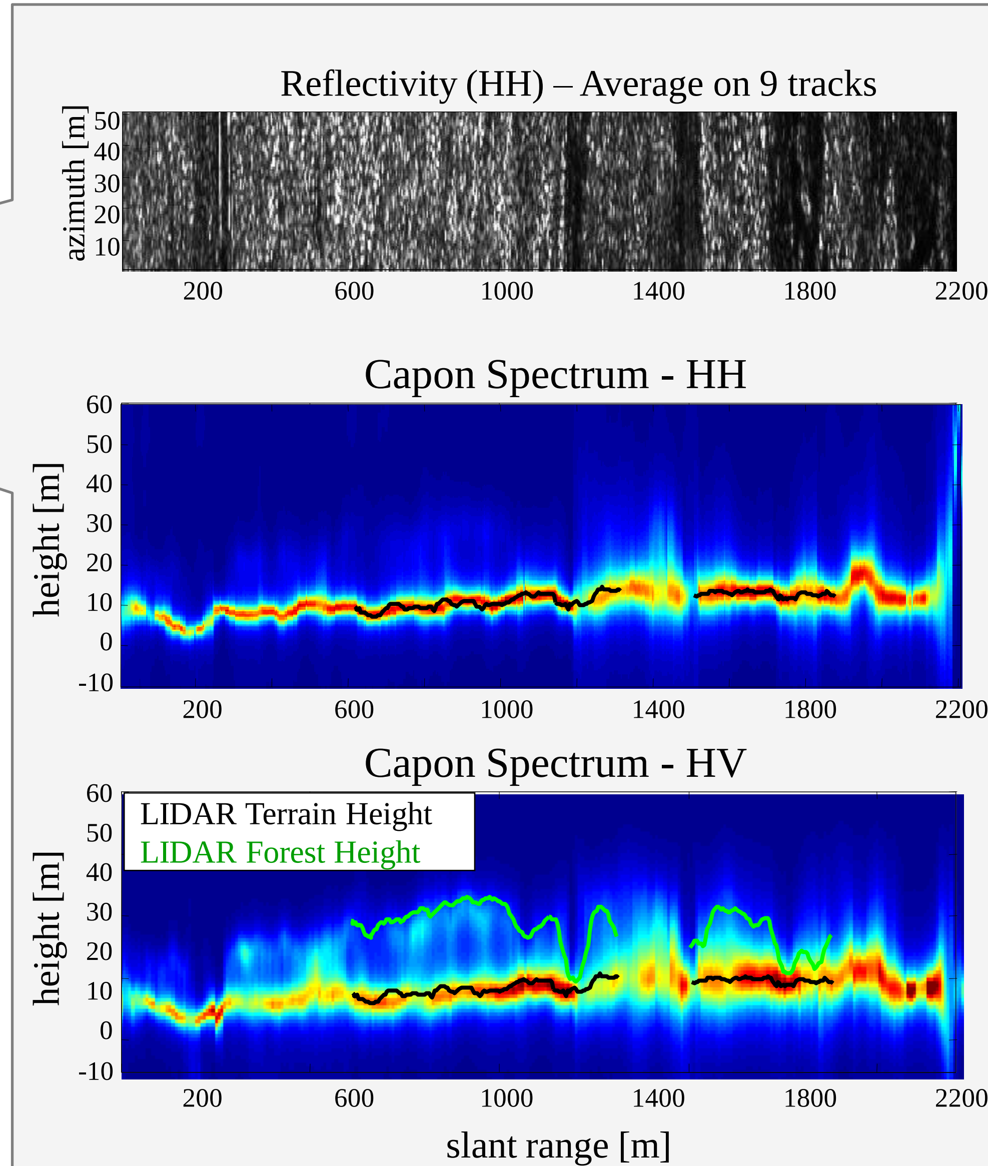

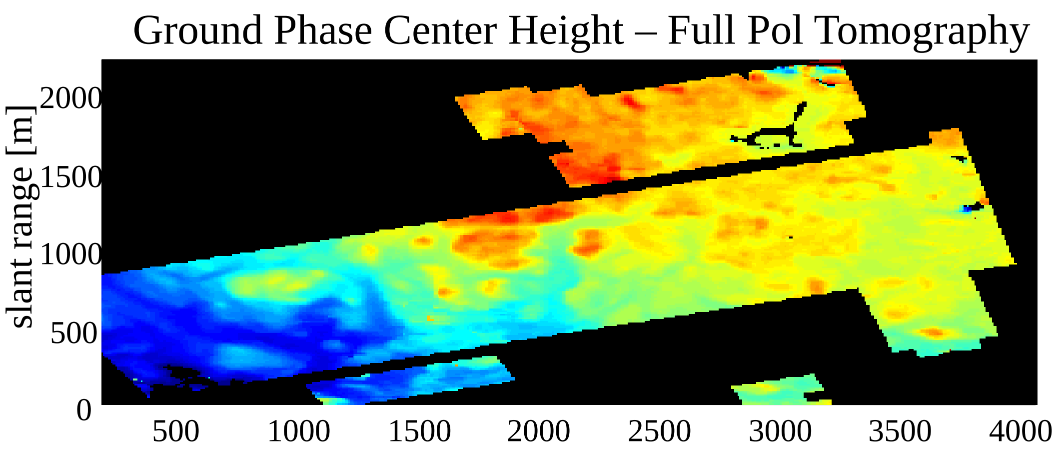

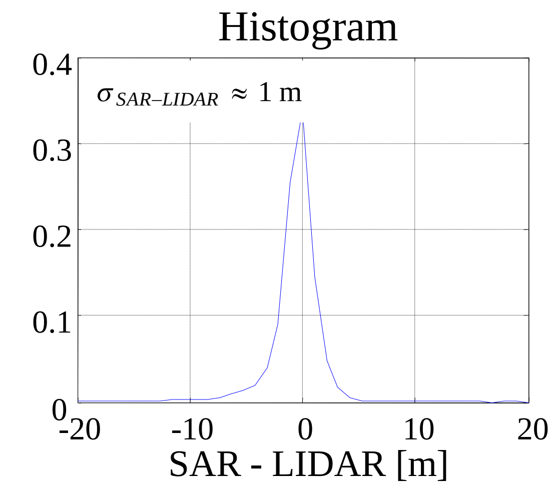

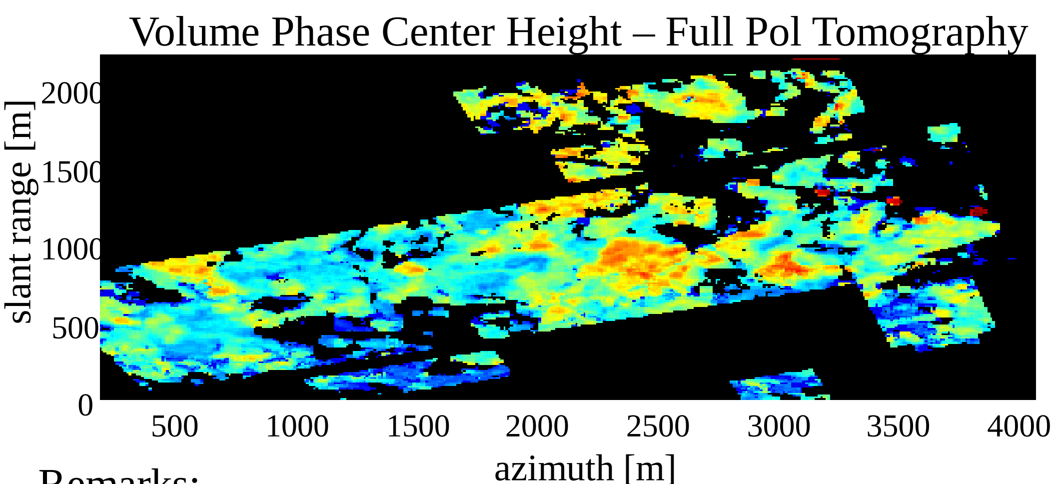

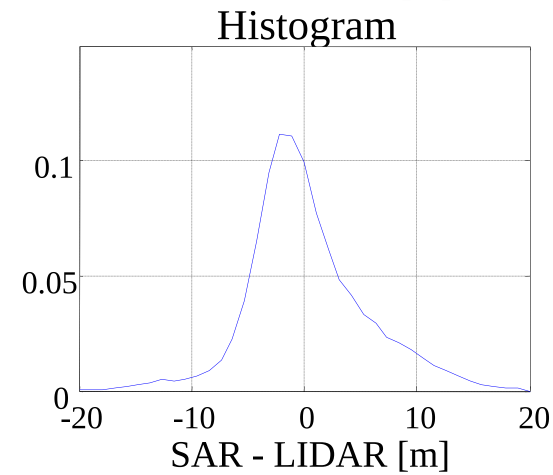

Remarks:

Phase center estimation is carried out through parametric estimation (*COMET*)

Full Pol Tomography is implemented by assuming that ground and volume phase center height is invariant with polarization

Examples from BioSAR 2007

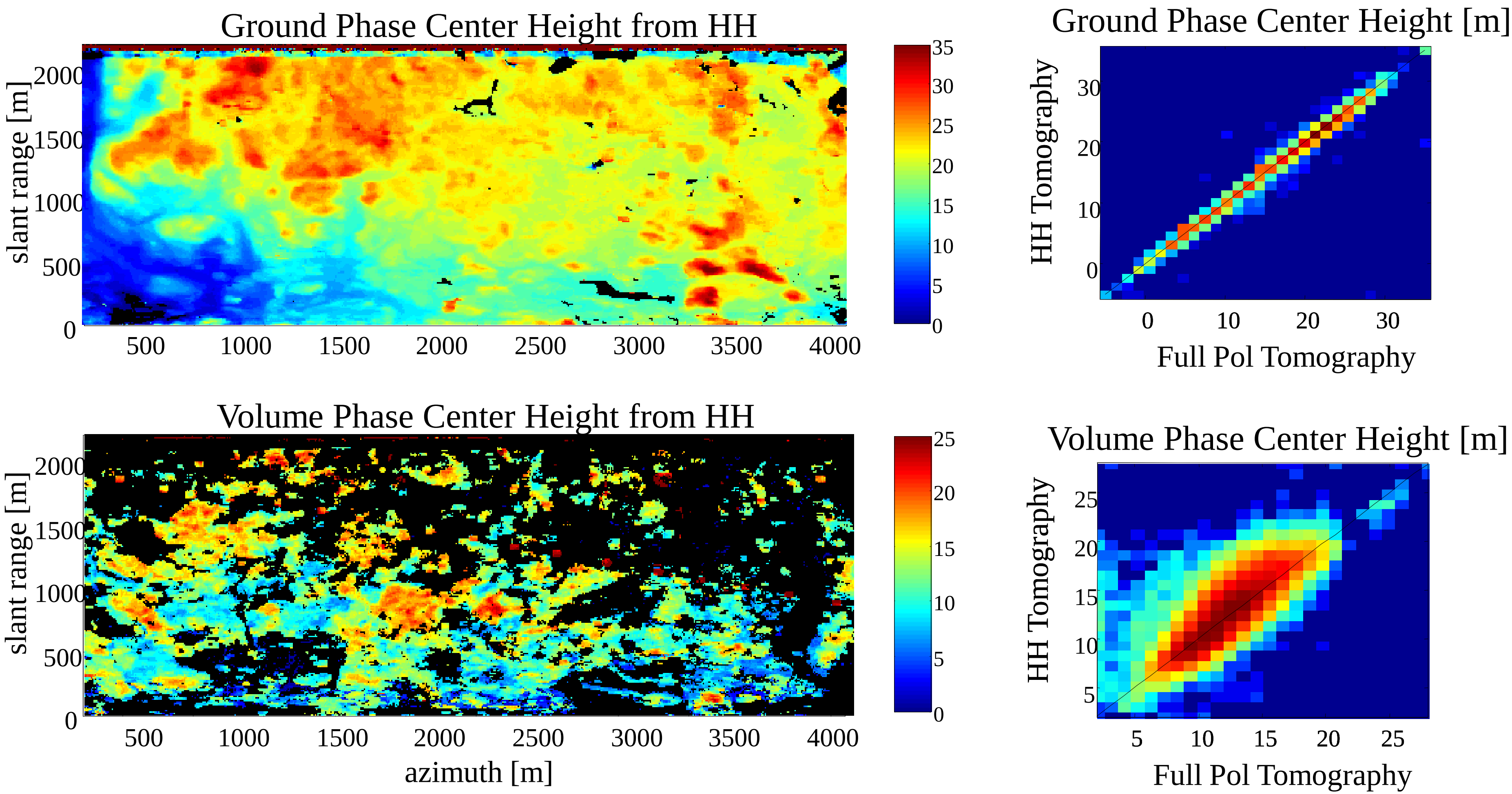

Examples from BioSAR 2007

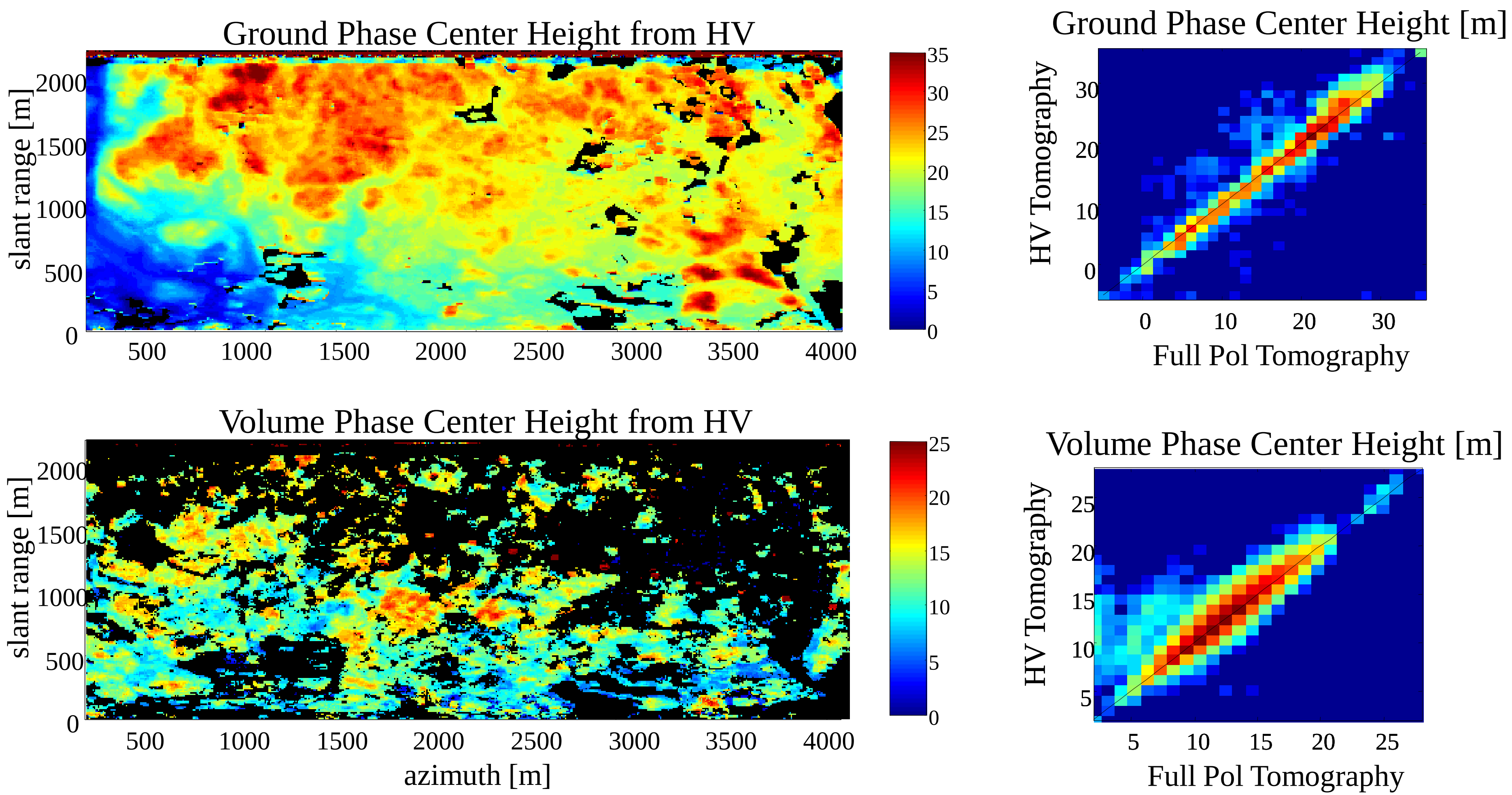

Remark: many open areas are sensed as noise in HV, consistently with the Small Perturbation Model

Examples from BioSAR 2007

Ground Phase Center Height from VV

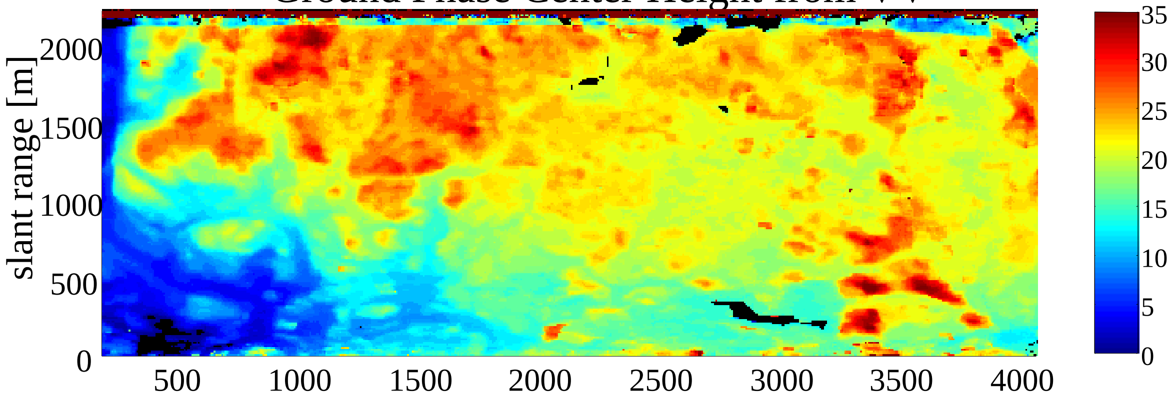

Ground Phase Center Height [m]

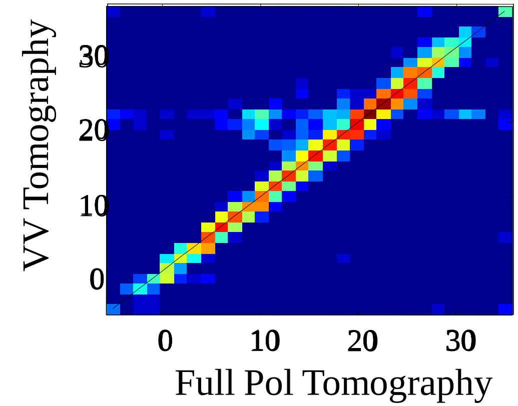

Volume Phase Center Height from VV

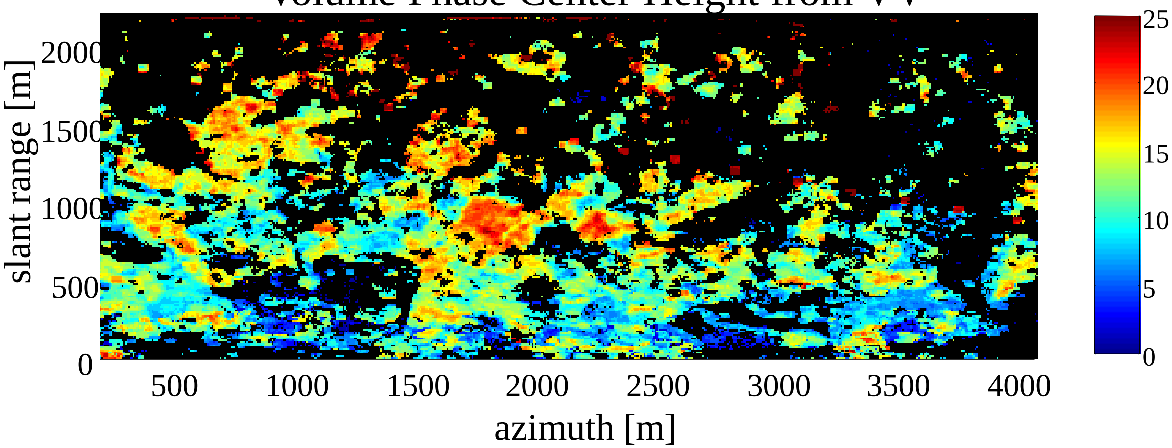

Volume Phase Center Height [m]

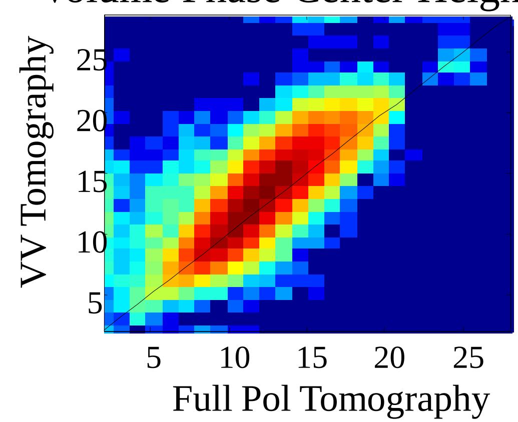

Remark: slightly higher volume phase center, consistent with the hypothesis of a higher extinction coefficient in VV

Campaign	TropiSAR- ESA
System	Sethi- ONERA
Period	August 2009
Site (among others)	Paracou, French Guyana
Scene	Tropical forest estimated 150 species per hectare Dominant families: Lecythidaceae, Leguminoseae, Chrysobalanaceae, Euphorbiaceae.
Tomographic tracks	6 – Fully Polarimetric
Carrier frequency	P-Band
Slant range resolution	≈1 m
Azimuth resolution	≈1 m
Vertical resolution	15 m

3D Imaging of the Guyaflux Tower

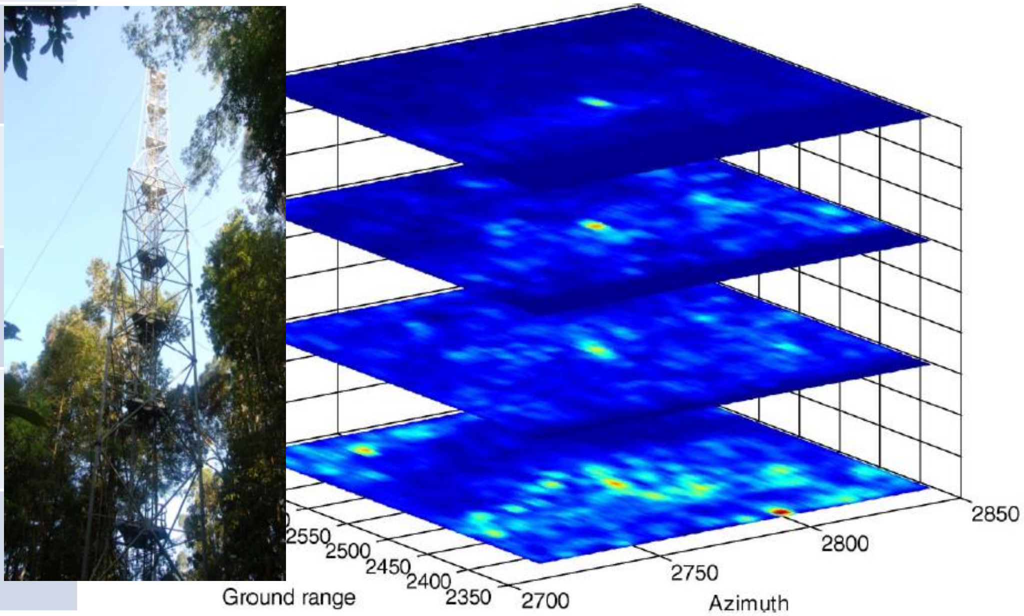

Examples from TropiSAR

Tomographic reconstruction of two azimuth cuts:

Method: coherent focusing

All panels have been re-interpolated such that the ground level corresponds to 0 m

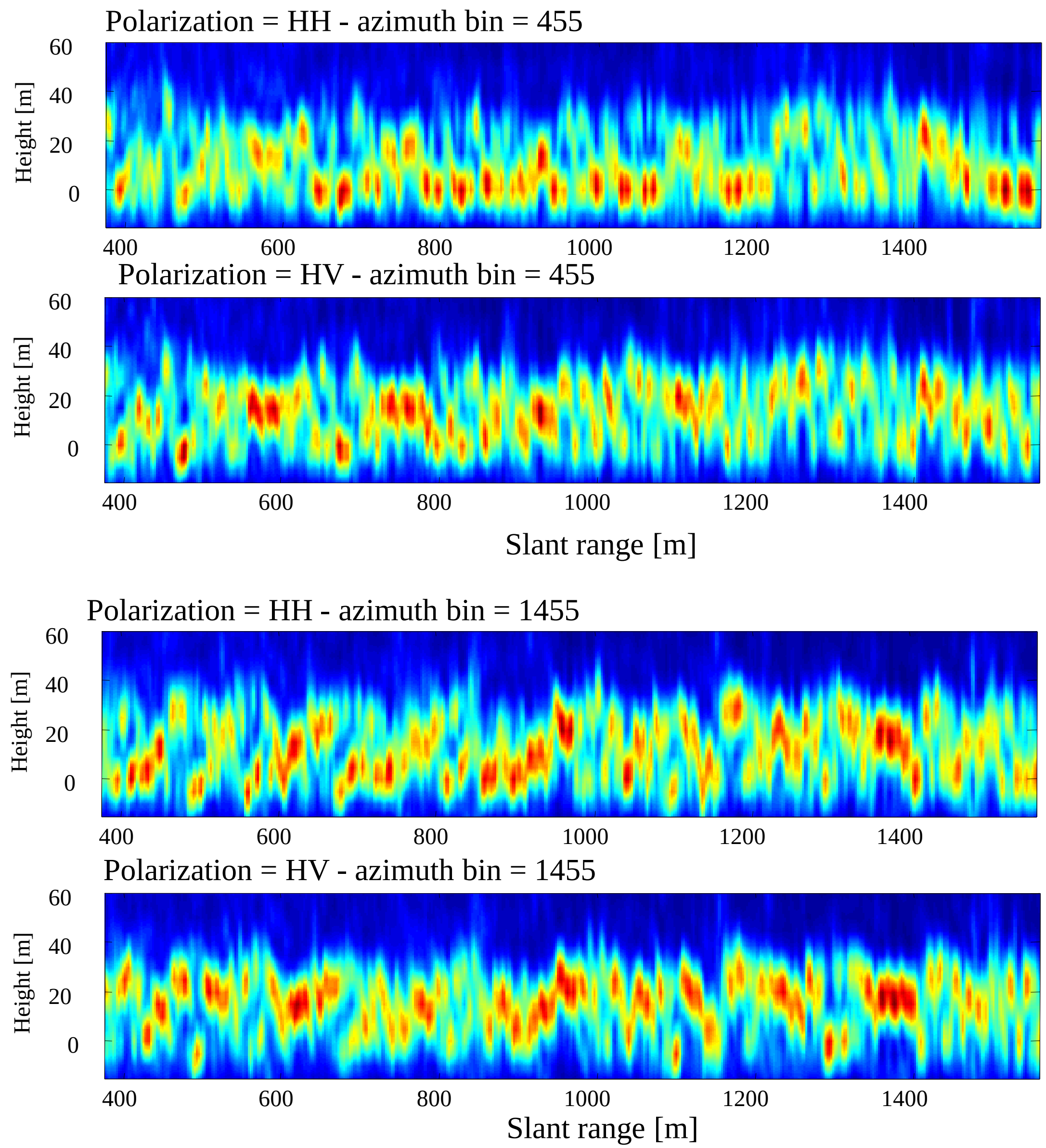

HH

Visible contribution from the ground level beneath the forest

Vegetation is well visible

HV

Poor contributions from the ground level beneath the forest

Vegetation is well visible

Tomographic reconstruction of radar scattering from four different heights

Method: coherent focusing

Polarization: HH

The strongest dependence on terrain topograpy is found at the ground level

The most uniform tomographic layer is found at about15-20 m above the ground

Highest layers exhibit a dependence on terrain topography, similarly to the ground layer

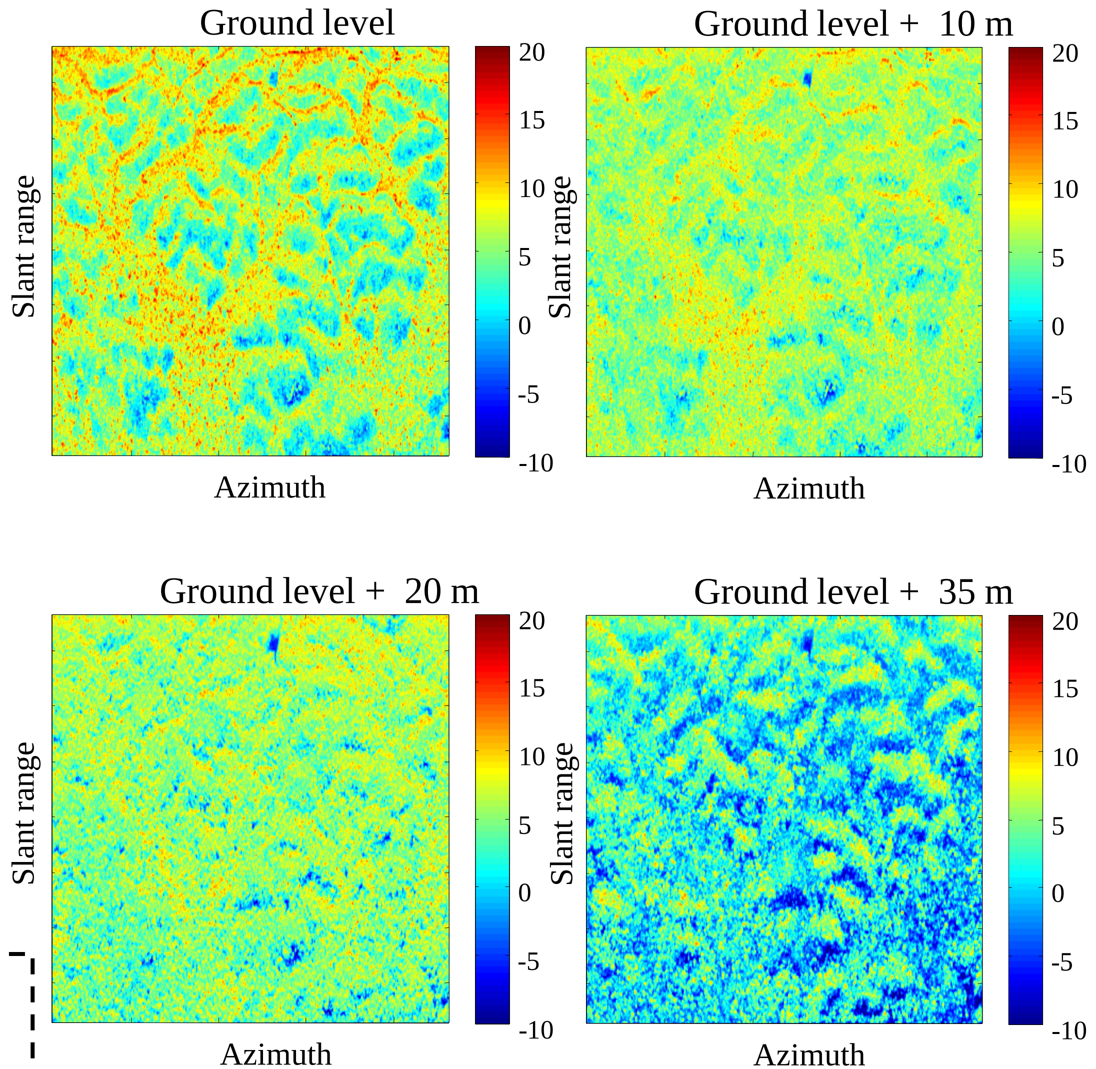

Tomographic data exhibit a more complex dependence of terrain topography than traditional SAR data.

A closer look…

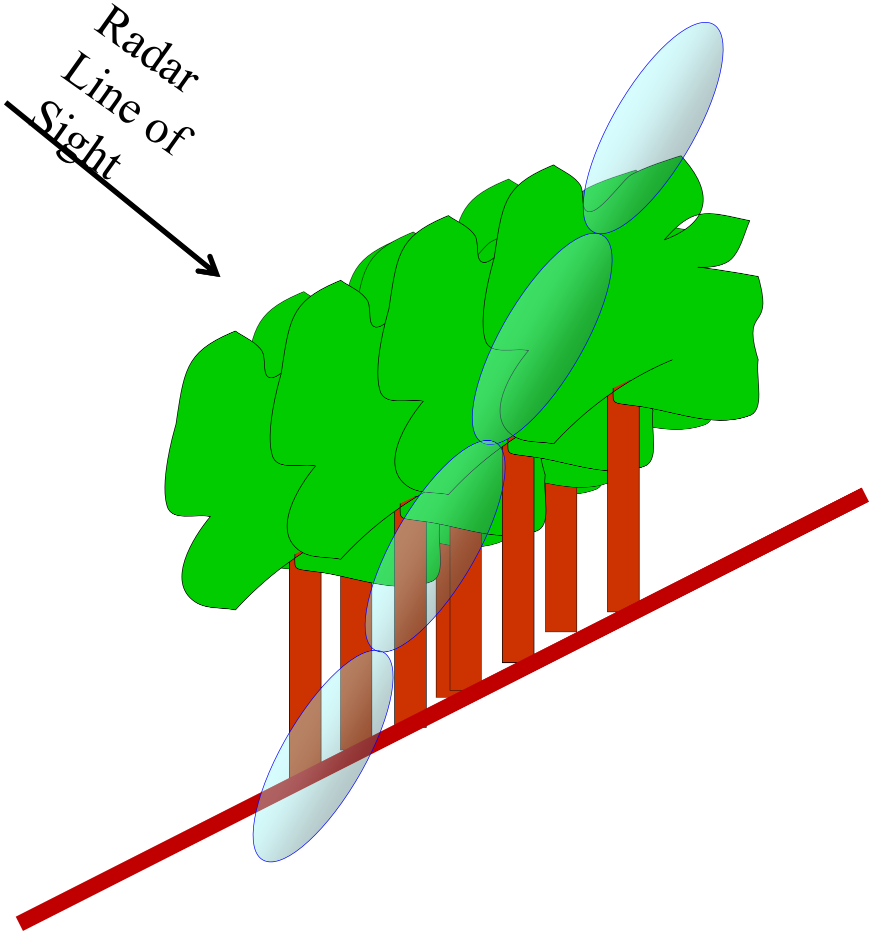

A closer look…

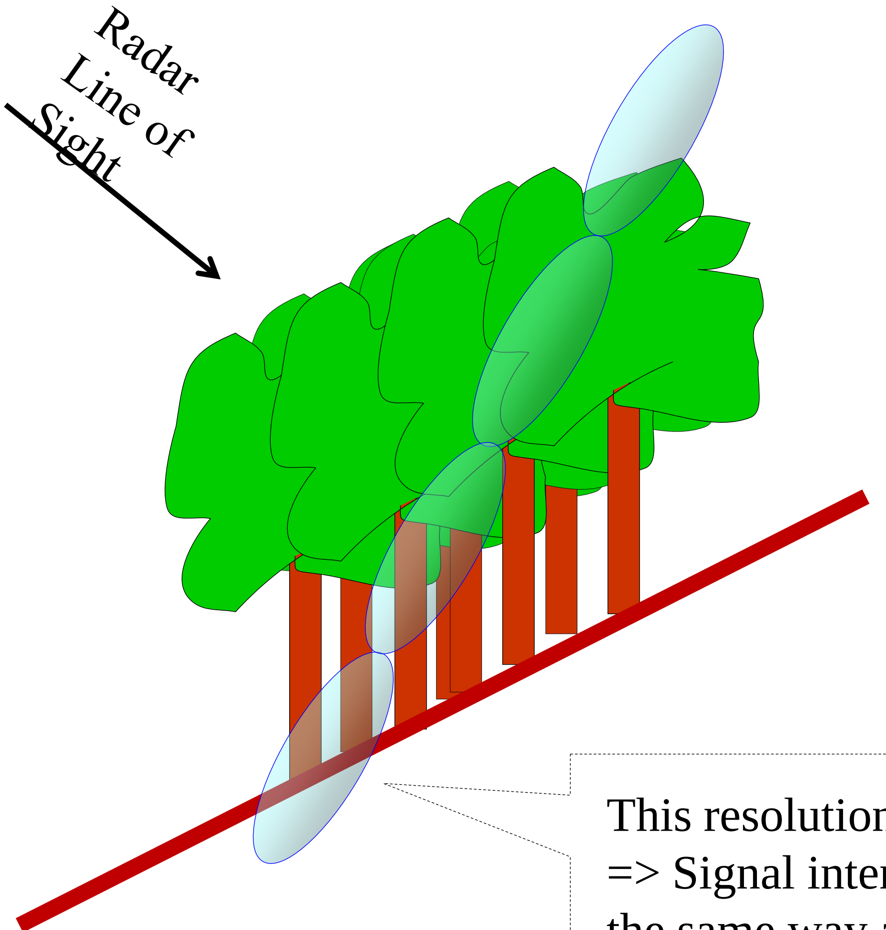

This resolution cell gathers contributions from terrain only.
=> Signal intensity in this cell is affected by terrain slope the same way as in traditional SAR images of bare surfaces

A closer look…

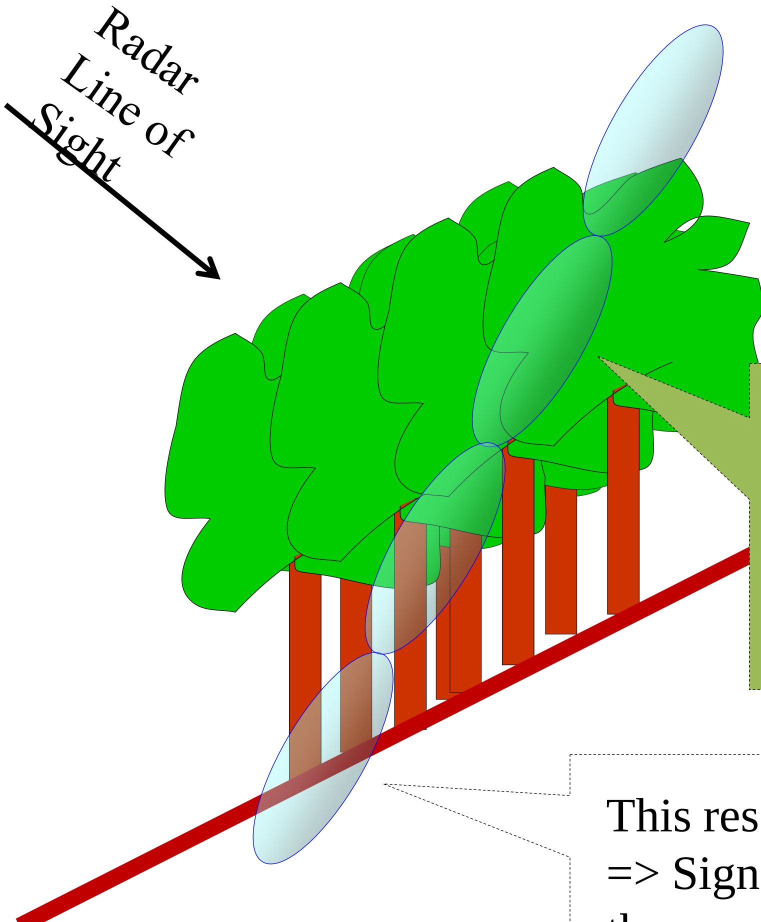

This cell is completely within the volume layer, independently on volume orientation w.r.t. the Radar LOS.
=> Signal intensity in this cell is independent of terrain slope

This resolution cell gathers contributions from terrain only.
=> Signal intensity in this cell is affected by terrain slope the same way as in traditional SAR images of bare surfaces

TROPISAR – Tomographic sections

A closer look…

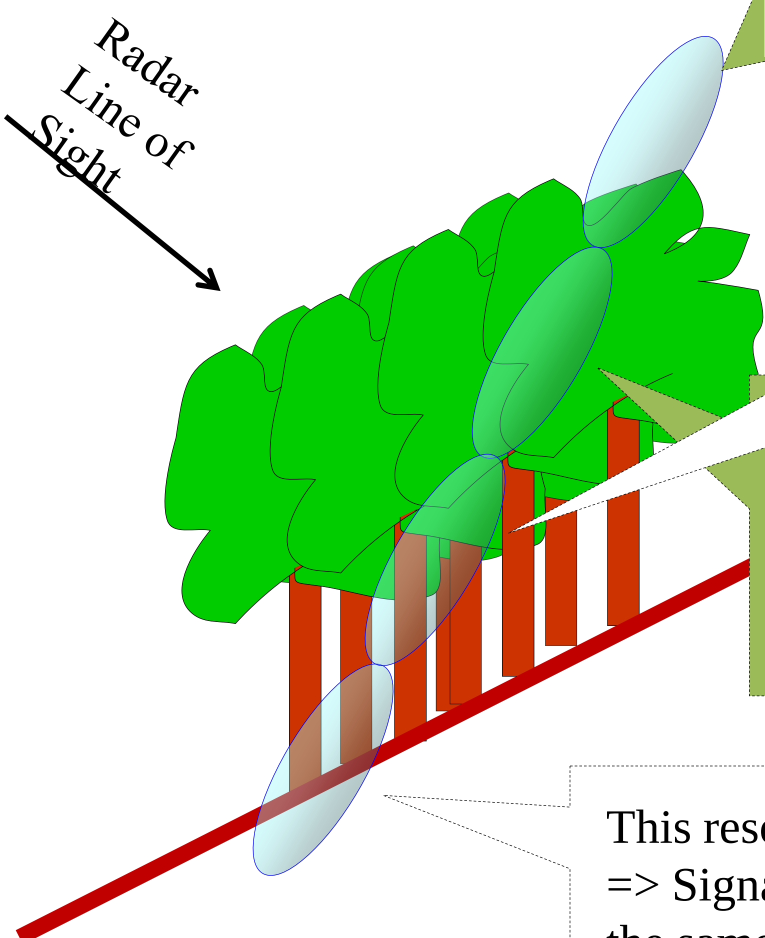

The scattering volume within cells at the boundaries of the vegetation layer depends on volume orientation w.r.t. the Radar LOS.
=> Signal intensity in this cell is affected by terrain slope in a similar way as the cell corresponding to the ground layer.

This cell is completely within the volume layer, independently on volume orientation w.r.t. the Radar LOS.
=> Signal intensity in this cell is independent of terrain slope

This resolution cell gathers contributions from terrain only.
=> Signal intensity in this cell is affected by terrain slope the same way as in traditional SAR images of bare surfaces

Examples from TropiSAR

Co-polar signature at the ground layer reveals ground-trunk double bounce interactions dominate the signal from flat areas *despite* the presence of a 40 m dense tropical forest

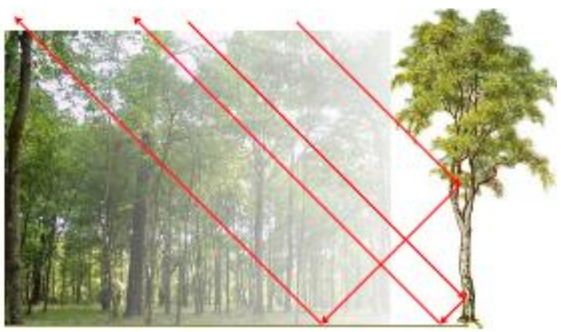

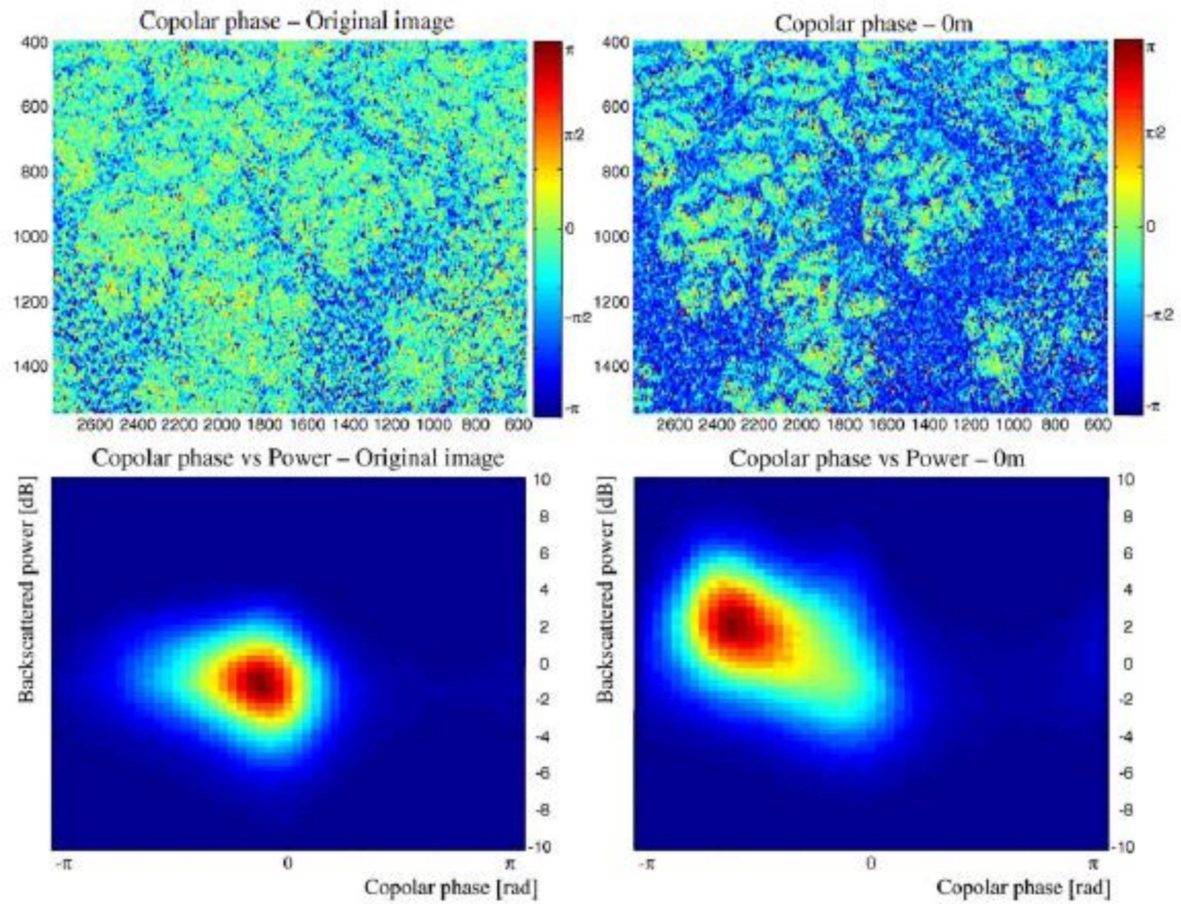

- TropiSCAT – ESA - 2011

  ⇔ a static ground-based radar observing a tropical forest

  - Located in French Guyana – same site as TropiSAR
  - Team members from ONERA, CNES, CESBIO, POLIMI
  - Automatic and systematic acquisition
  - Fully polarimetric (HH, HV, VH and VV)
  - Tomographic capability (to have a vertical discrimination of backscattering mechanisms)
  - Coupled with geophysical parameters measurements (provided by INRA – National Institute for Agronomic Research)
  - **GOAL: provide continuous observations (15 mn sampling) over a time span of one year**

Examples from TropiSCAT

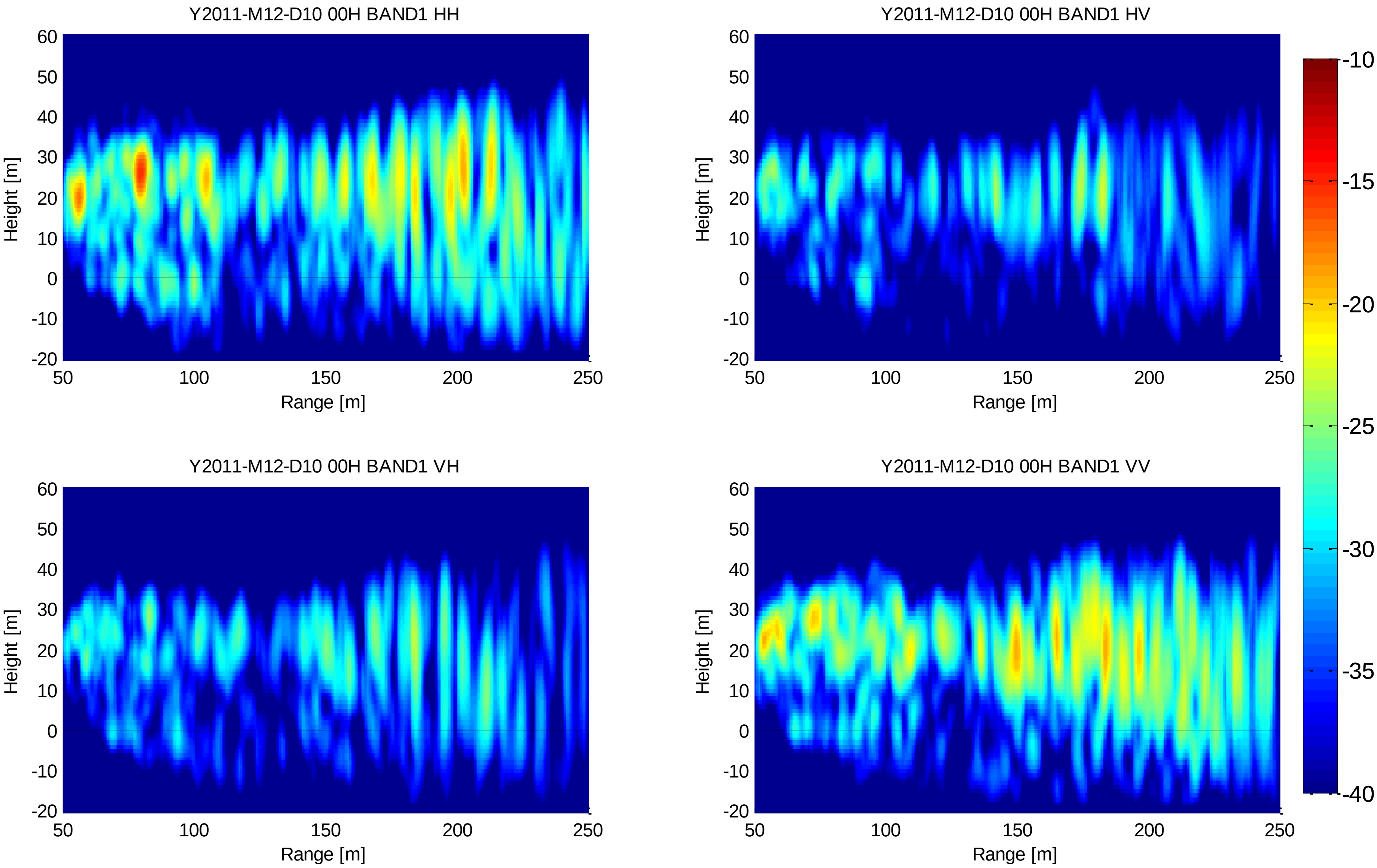

Outline

Introduction to SAR Tomography

- Basic Concepts
- Tomographic Scene Reconstruction
- Polarimetry and Tomography: Examples

Optimization Methods

- Multi-layer Optimization
- Multi-baseline Coherence Optimization

Ground-volume Decomposition

- Problem Statement
- SKP Structure
- SKP Decomposition
- Regions of Physical Validity
- Boundary Solutions
- Case Studies

Conclusions

MB PolInSAR

Vertical resolution ≈ 1 ÷ 15 m
N ≈ 6 ÷ 50

Vertical resolution ≈ 10 ÷ 30 m
N ≈ 6 ÷ 15

Vertical resolution >> 30 m
N ≥ 2

Single Baseline PolInSAR
N = 2

Multi-layer Optimization

The analysis so far has been limited to the comparison of Tomographic results from different polarizations

Further information can be extracted by *jointly* exploiting baseline and polarization diversity

Multi-layer optimization techniques do this by finding the *optimum* polarization for *each* layer:

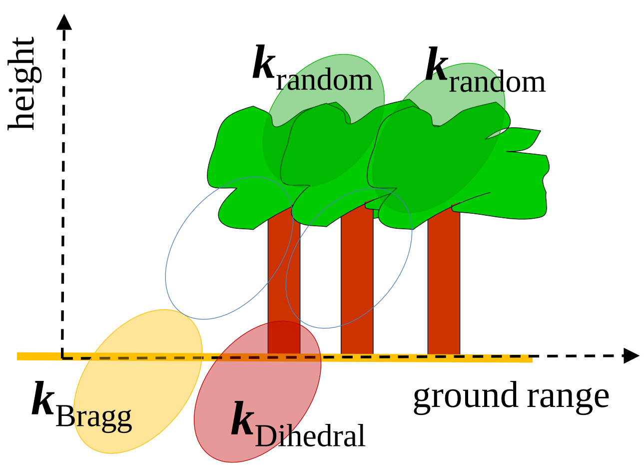

Two benefits:

- Enhanced classification capabilities
- Tomographic resolution is improved

Multi-layer optimization techniques extend single-pol Spectral Estimators by considering the data covariance matrix among all tracks *and* all polarizations

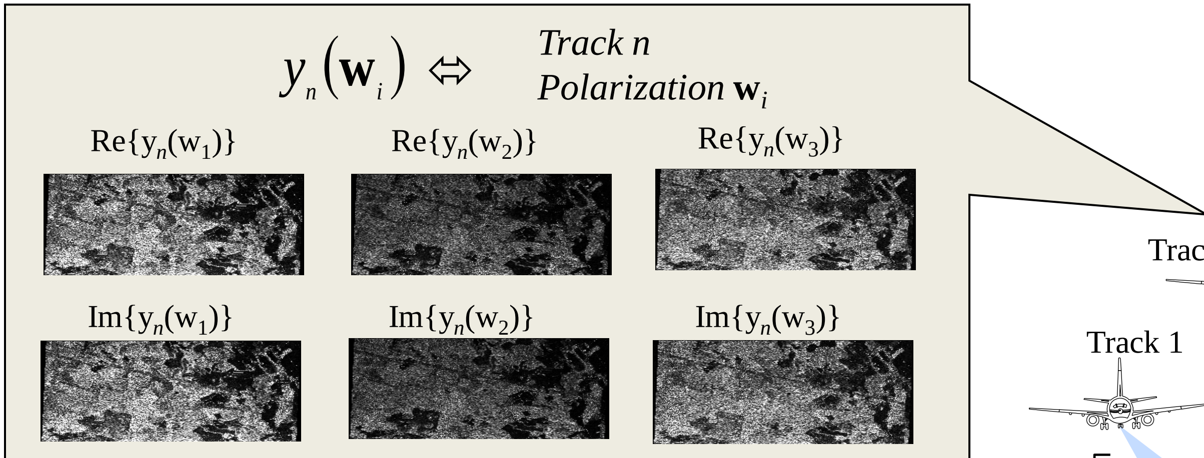

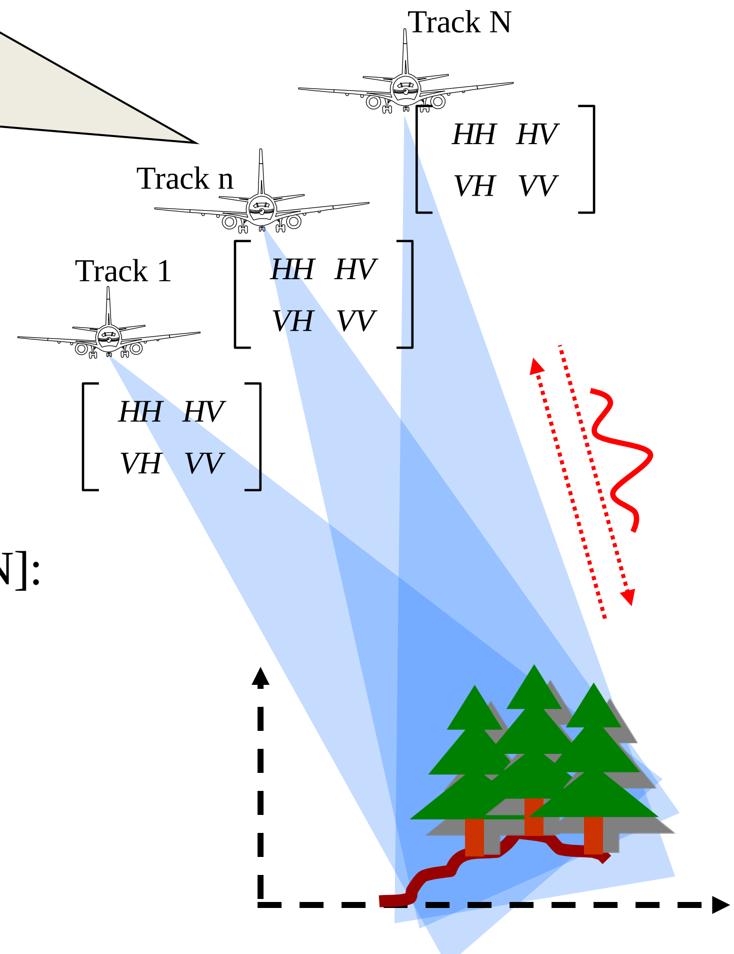

Data vector [3Nx1]:

$$\mathbf{y} = \begin{bmatrix} \mathbf{y}_{MB}(\mathbf{w}_1) \\ \mathbf{y}_{MB}(\mathbf{w}_2) \\ \mathbf{y}_{MB}(\mathbf{w}_3) \end{bmatrix} \Rightarrow$$

Data covariance matrix [3Nx3N]:

$$\mathbf{W} = E\left[\mathbf{y}\mathbf{y}^H\right] = \begin{bmatrix} \mathbf{R}_{11} & \mathbf{R}_{12} & \mathbf{R}_{13} \\ \mathbf{R}_{21} & \mathbf{R}_{22} & \mathbf{R}_{23} \\ \mathbf{R}_{31} & \mathbf{R}_{32} & \mathbf{R}_{33} \end{bmatrix}$$

Multi-layer optimization techniques extend single-pol Spectral Estimators by considering the data covariance matrix among all tracks *and* all polarizations

In most cases, the extension from single-pol to multi-pol is simply obtained through an eigenvalue problem

Beamforming

$$\hat{S}(v) = \mathbf{a}^H(v)\hat{\mathbf{R}}\mathbf{a}(v)$$

$$\hat{S}_{MP}(v) = \max_{\mathbf{k}} \left\{ \mathbf{k}^H \left(\mathbf{B}^H(v)\hat{\mathbf{W}}\mathbf{B}(v) \right) \mathbf{k} \right\}$$

$$\Leftrightarrow \left(\mathbf{B}^H(v)\hat{\mathbf{W}}\mathbf{B}(v) \right) \mathbf{k}_{opt} = \lambda_{\max} \mathbf{k}_{opt}$$

$$\mathbf{B}(v) = \begin{bmatrix} \mathbf{a}(v) & 0 & 0 \\ 0 & \mathbf{a}(v) & 0 \\ 0 & 0 & \mathbf{a}(v) \end{bmatrix}$$

Capon Estimator

$$\hat{S}(v) = \left(\mathbf{a}^H(v)\hat{\mathbf{R}}^{-1}\mathbf{a}(v) \right)^{-1}$$

$$\hat{S}_{MP}(v) = \max_{\mathbf{k}} \left\{ \left(\mathbf{k}^H \left(\mathbf{B}^H(v)\hat{\mathbf{W}}^{-1}\mathbf{B}(v) \right) \mathbf{k} \right)^{-1} \right\}$$

$$\Leftrightarrow \left(\mathbf{B}^H(v)\hat{\mathbf{W}}^{-1}\mathbf{B}(v) \right) \mathbf{k}_{opt} = \lambda_{\min} \mathbf{k}_{opt}$$

Example: Separation of two closely spaced scattering centers

Simulated Backscattered Power Distribution (BPD)

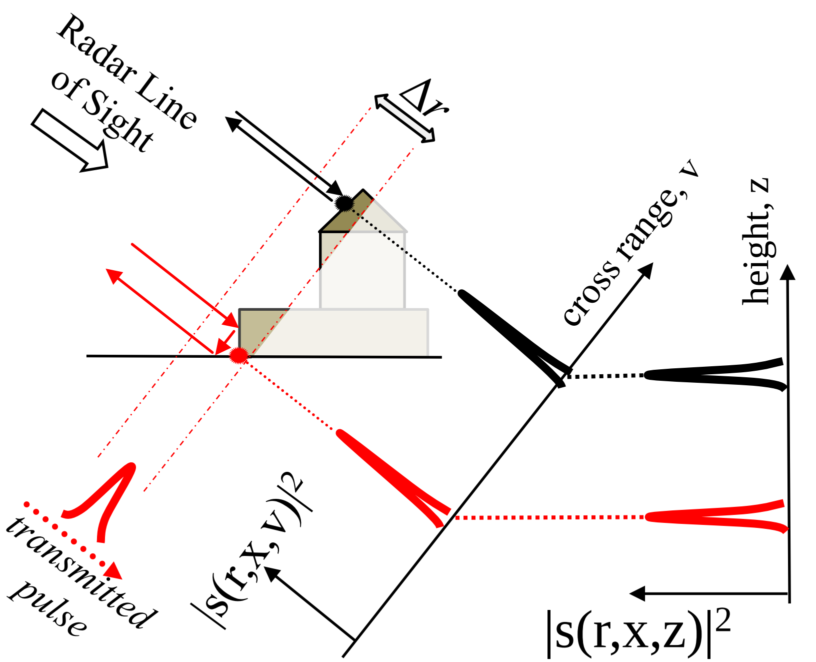

Double Bounce Scattering (Dihedral)

Single Bounce Scattering (Trihedral)

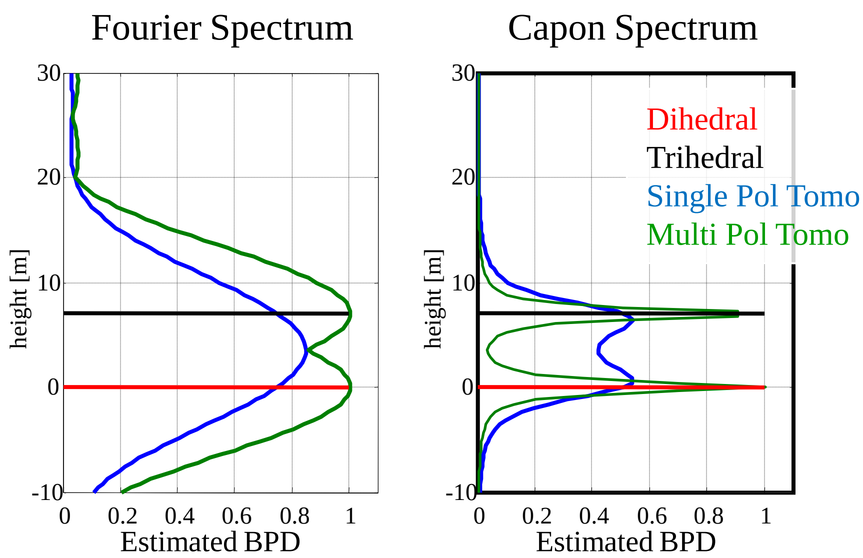

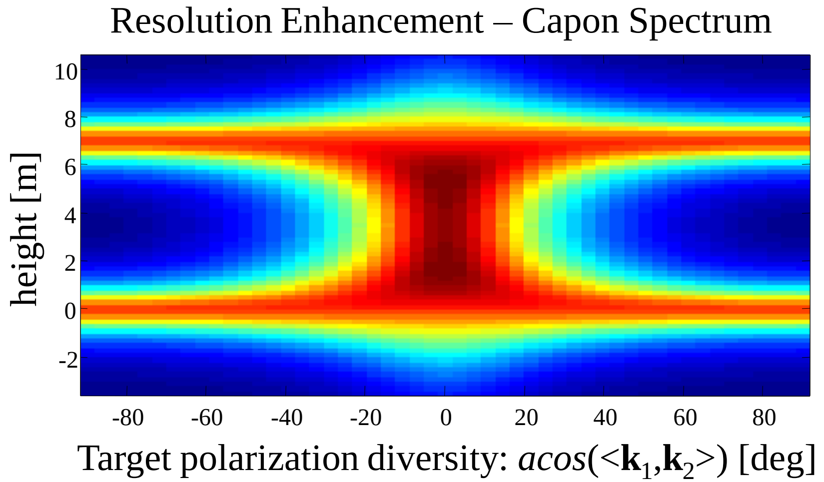

A real world example: imaging of a truck under the foliage

From: Y. Huang, L. Ferro-Famil, A. Reigber, "Under Foliage Object Imaging Using SAR Tomography and Polarimetric Spectral Estimators," Eusar 2010 – Courtesy of the authors

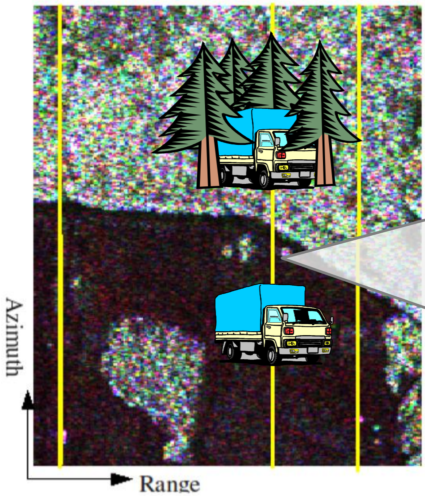

System	E-SAR – DLR
Site	Dornstetten, Germany
Tomographic tracks	21 – Fully Polarimetric
Carrier frequency	L-Band
Vertical resolution	2 m

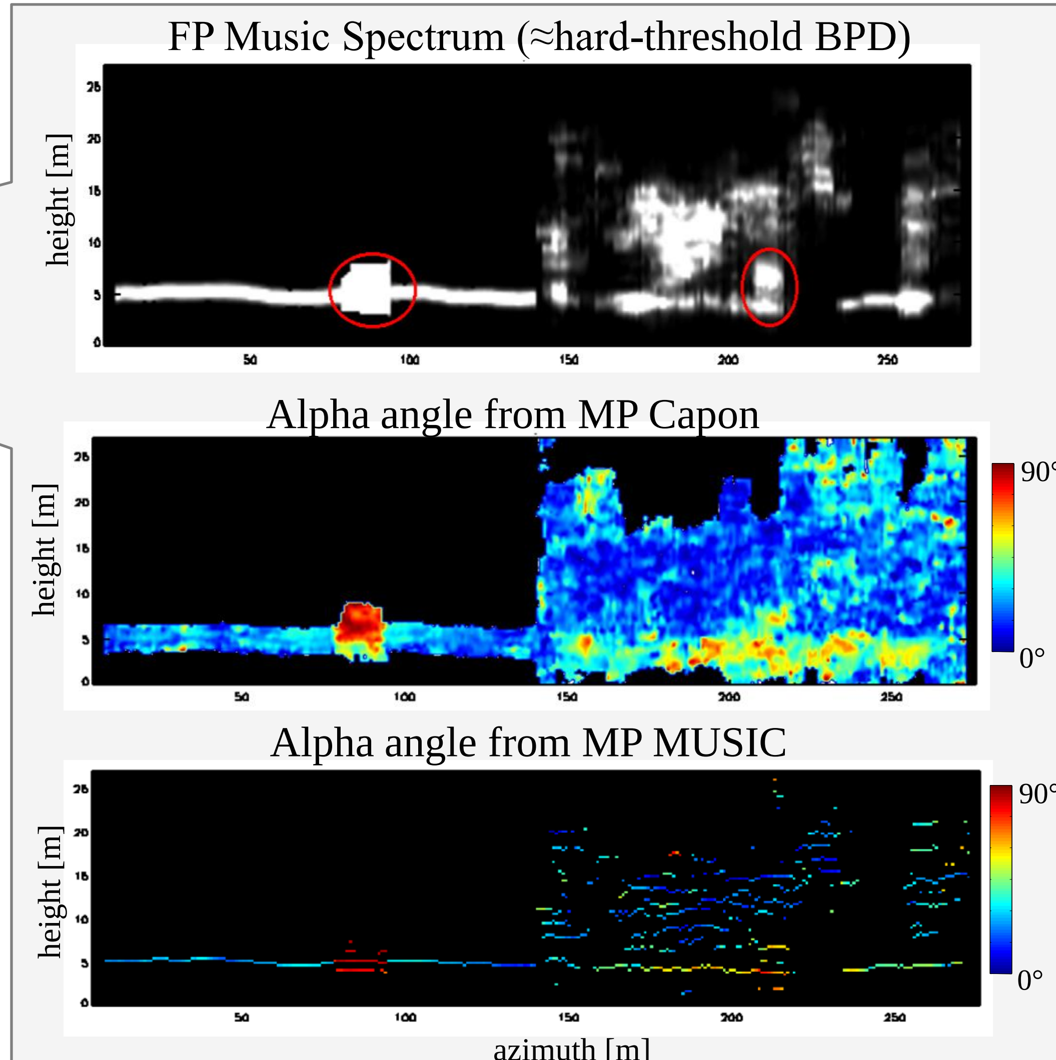

Multi-baseline Coherence Optimization

Coherence optimization enhances InSAR capabilities by allowing the analysis of multiple targets with different polarimetric responses within the same resolution cell

Example: resolving three closely spaced point scatterers

The interferometric coherences associated with the three points alone are obtained by optimizing w.r.t. the projection vector:

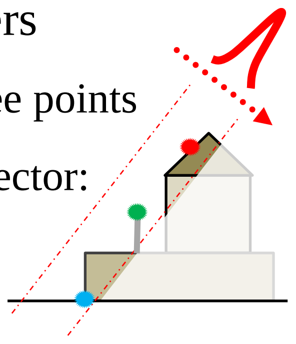

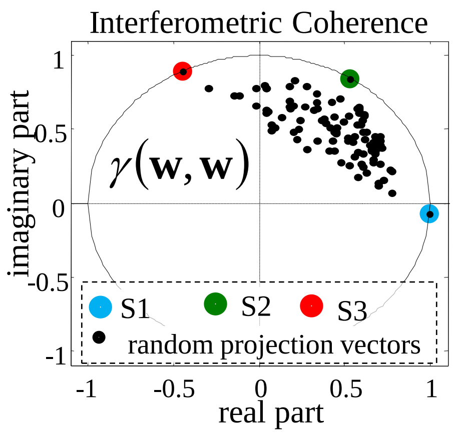

$$\gamma(S_k) = \gamma\left(\mathbf{w}_{opt}^{(k)}, \mathbf{w}_{opt}^{(k)}\right)$$

$$\mathbf{w}_{opt}^{(k)} = \arg\max\{\gamma(\mathbf{w},\mathbf{w})\}$$

where:

$$\gamma(\mathbf{w}_i,\mathbf{w}_j) = \frac{E\left[y_n(\mathbf{w}_i)y_m^*(\mathbf{w}_j)\right]}{\sqrt{E\left[\left|y_n(\mathbf{w}_i)\right|^2\right]E\left[\left|y_m(\mathbf{w}_j)\right|^2\right]}}$$

Multi-baseline Coherence Optimization

Coherence optimization enhances InSAR capabilities by allowing the analysis of multiple targets with different polarimetric responses within the same resolution cell

MB coherence optimization methods simultaneously optimize coherences in several baselines. Thus, they are expected to deliver more robust estimates:

Two approaches are considered:

Multiple Scattering Mechanisms (MSM)

A distinct SM is assigned to each track.

$$\max\left\{\sum_{n=1}^{N}\sum_{\substack{m=1\\m\neq n}}^{N}\left|\gamma_{nm}\left(\mathbf{w}_n,\mathbf{w}_m\right)\right|\right\}:\angle\mathbf{w}_n^H\mathbf{w}_m=0$$

- Fit for SMs that might have different polarimetric signatures in different tracks
- Robust to miscalibration

Equalized Scattering Mechanism (ESM)

Enforces equal polarimetric signatures of scatterers along all baselines

$$\max\left\{\sum_{n=1}^{N}\sum_{\substack{m=1\\m\neq n}}^{N}\left|\gamma_{nm}\left(\mathbf{w},\mathbf{w}\right)\right|\right\}$$

- Implies data stationarity
- Leads to lower coherence magnitudes,
- Processes all available information by enforcing more constraints, and thus more accurately

A real world example: MB coherence optimization

From M. Neumann, L. Ferro-Famil, A. Reigber: "Multibaseline Polarimetric SAR Interferometry Coherence Optimization", IEEE Geoscience and Remote Sensing Letters, 2008 – Courtesy of the authors

Coherence between passages 1 and 2 associated with the dominant SM

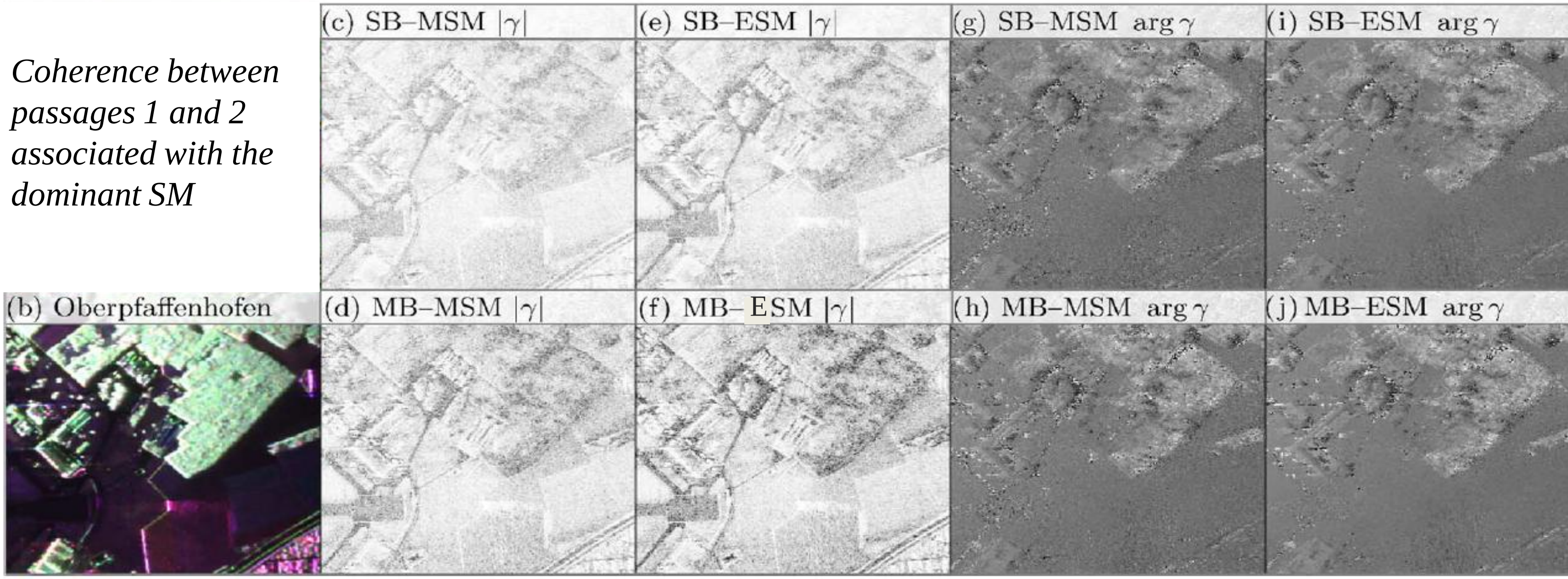

System	**E-SAR – DLR**
Site	Oberpfafenhoffen, Germany
Scene	Forests, surface, and urban areas
Tracks	5 – Fully Polarimetric
Carrier frequency	L-Band

Remarks:
SB optimized coherences achieve higher values than MB

Relevant contrast improvement of MB over SB, particularly over forested areas.

Outline

Introduction to SAR Tomography

- Basic Concepts
- Tomographic Scene Reconstruction
- Polarimetry and Tomography: Examples

Optimization Methods

- Multi-layer Optimization
- Multi-baseline Coherence Optimization

Ground-volume Decomposition

- Problem Statement
- SKP Structure
- SKP Decomposition
- Regions of Physical Validity
- Boundary Solutions
- Case Studies

Conclusions

MB PolInSAR

Vertical resolution ≈ 1 ÷ 15 m
N ≈ 6 ÷ 50

Vertical resolution ≈ 10 ÷ 30 m
N ≈ 6 ÷ 15

Vertical resolution >> 30 m
N ≥ 2

Single Baseline PolInSAR
N = 2

Problem Statement

Decompose the data covariance matrix into ground-only and volume-only contributions

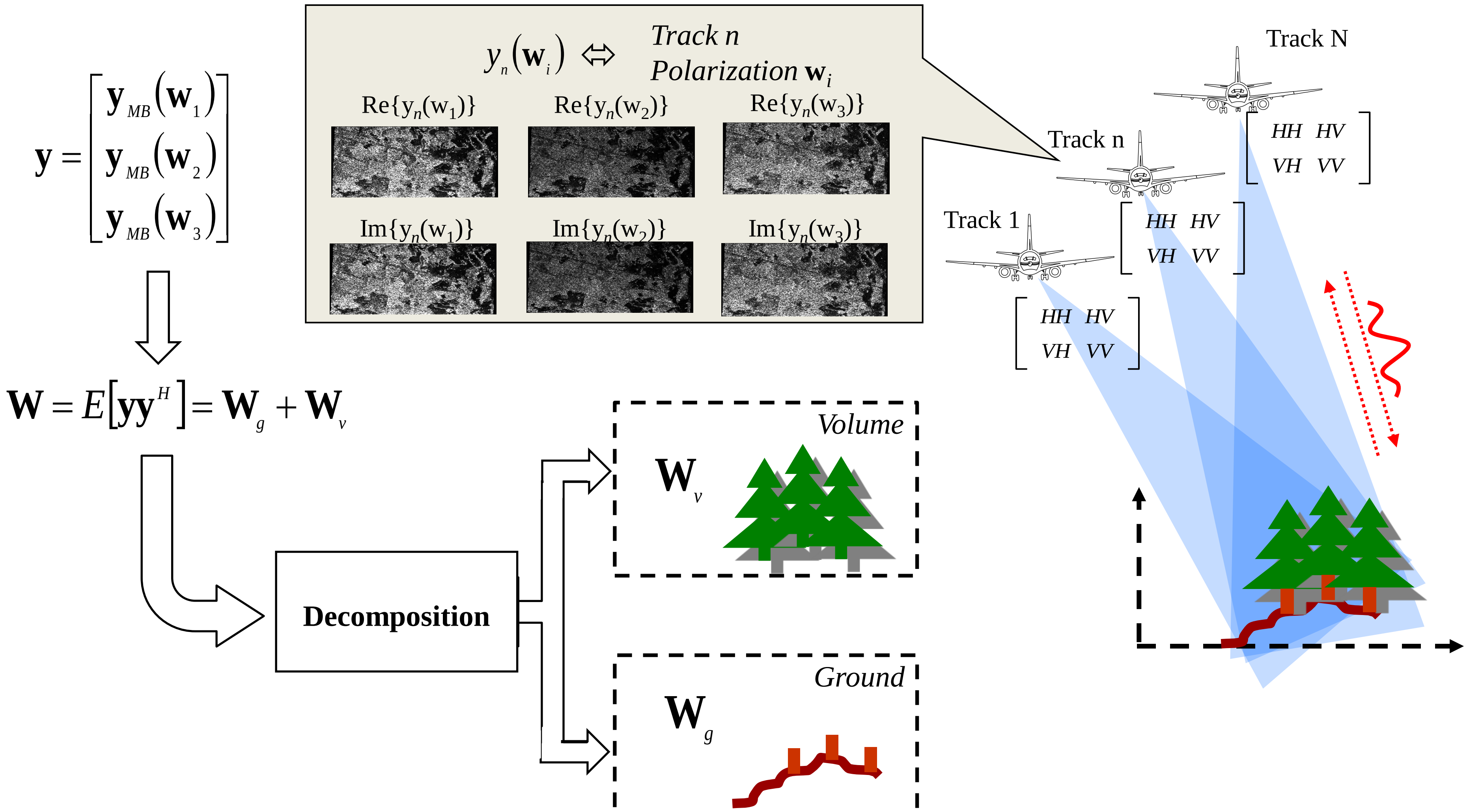

Ground-volume decomposition implies:

- Separation of Structural Properties

  => Separated Tomographic Imaging of Ground-only and Volume-only Contributions

HV

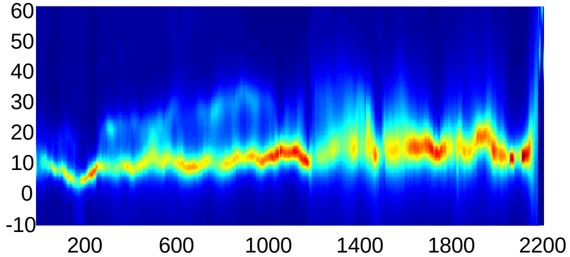

Ground

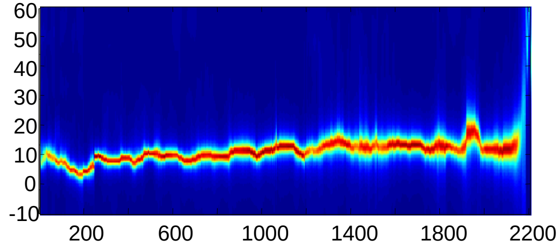

Volume

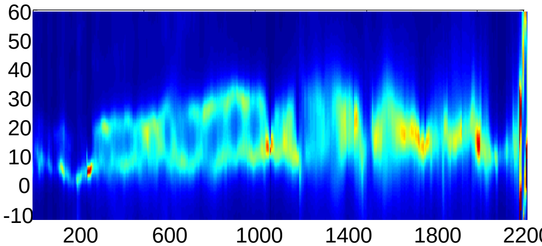

- Separation of Polarimetric Properties

  => Evaluation of the Ground to Volume Backscattered Power Ratio for each polarization

P-Band HH

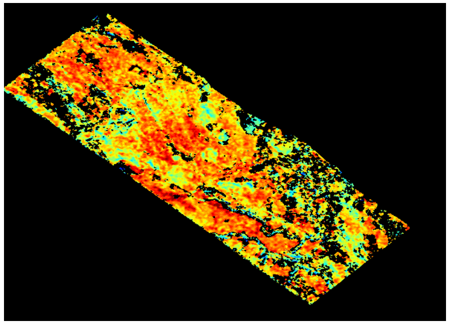

P-Band HV

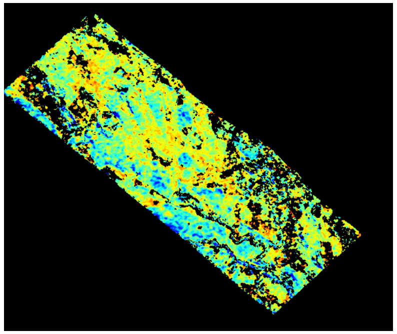

L-Band HH

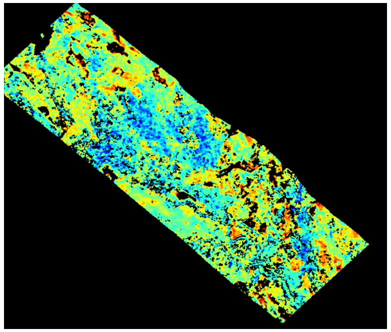

L-Band HV

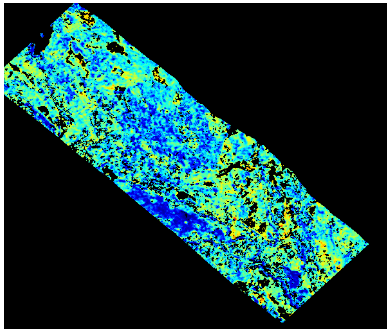

SKP Structure

Without loss of generality, the received signal can be assumed to be contributed by *K* distinct Scattering Mechanisms (SMs), representing ground, volume, ground-trunk scattering, or other

$$y_n(\mathbf{w}_i) = \sum_{k=1}^{K} s_k(n;\mathbf{w}_i)$$

$s_k(n, \mathbf{w}_\mathrm{i})$: contribution of the *k-th* SM in Track *n*, Polarization $\mathbf{w}_\mathrm{i}$

Three fundamental hypotheses will be retained:

H1): **Statistical independence** among different SMs

H2): **Invariance of the interferometric coherences** of **each** SM w.r.t. polarization

$\Rightarrow$ negligible variation of the EM properties of each SM (subsurface penetration, volume extinction,…) w.r.t. polarization

H3): **Invariance of the polarimetric signature** of **each** SM on the choice of the track

$\Rightarrow$ events like floods, fires, frosts, are expected **not** to occur during the acquisition campaign

H1) H2) H3) $\Rightarrow$

$$E\left[y_n(\mathbf{w}_i)\, y_m^*(\mathbf{w}_j)\right] = \sum_{k=1}^{K} c_k(\mathbf{w}_i, \mathbf{w}_j) \cdot \gamma_k(n,m)$$

$c_k(\mathbf{w}_\mathrm{i},\mathbf{w}_\mathrm{j})$: polarimetric correlation of the *k-th* SM in polarizations $\mathbf{w}_\mathrm{i}$,$\mathbf{w}_\mathrm{j}$

$$c_k(\mathbf{w}_i, \mathbf{w}_j) = E\left[s_k(n;\mathbf{w}_i)\, s_k^*(m;\mathbf{w}_j)\right]$$

γ_k(n,m) : interferometric coherence of the *k-th* SM in the *nm-th* interferogram

$$\gamma_k(n,m) = \frac{E\left[s_k(n;\mathbf{w}_i)\, s_k^*(m;\mathbf{w}_j)\right]}{\sqrt{E\left[\left|s_k(n;\mathbf{w}_i)\right|^2\right] E\left[\left|s_k(m;\mathbf{w}_j)\right|^2\right]}}$$

The same result is expressed in matrix form as a Sum of Kronecker Products (SKP)

$$E\left[y_n(\mathbf{w}_i)y_m^*(\mathbf{w}_j)\right] = \sum_{k=1}^{K} c_k(\mathbf{w}_i, \mathbf{w}_j)\cdot\gamma_k(n,m) \Leftrightarrow \mathbf{W} = E\left[\mathbf{y}\mathbf{y}^H\right] = \sum_{k=1}^{K} \mathbf{C}_k \otimes \mathbf{R}_k$$

Each SM is represented by a Kronecker Product (KP) of two matrices:

Polarimetric Signature, $\mathbf{C}_k$:

polarimetric covariance matrix of the *k-th* SM **alone** [3 x 3]

⇔ Electromagnetic properties of the *k-th* SM

$$\mathbf{C}_k = \begin{bmatrix} c_k(\mathbf{w}_1,\mathbf{w}_1) & c_k(\mathbf{w}_1,\mathbf{w}_2) & c_k(\mathbf{w}_1,\mathbf{w}_3) \\ c_k(\mathbf{w}_2,\mathbf{w}_1) & c_k(\mathbf{w}_2,\mathbf{w}_2) & c_k(\mathbf{w}_2,\mathbf{w}_3) \\ c_k(\mathbf{w}_3,\mathbf{w}_1) & c_k(\mathbf{w}_3,\mathbf{w}_2) & c_k(\mathbf{w}_3,\mathbf{w}_3) \end{bmatrix}$$

Structure Matrix, $\mathbf{R}_k$:

matrix of the interferometric coherences of the *k-th* SM **alone** [N x N]

⇔ Backscattered power distribution of the *k-th* SM

$$\mathbf{R}_k = \begin{bmatrix} \gamma_k(1,1) & \gamma_k(1,2) & \cdots & \gamma_k(1,N) \\ \gamma_k(2,1) & \gamma_k(2,2) & & \gamma_k(2,N) \\ \vdots & & \ddots & \vdots \\ \gamma_k(N,1) & \gamma_k(N,2) & \cdots & \gamma_k(N,N) \end{bmatrix}$$

$\mathbf{R}_k$, $\mathbf{C}_k$ are (semi)positive definite by definition

SKP Decomposition

SKP Decomposition = *fast* technique for the decomposition of *any* matrix into a SKP

W ⟹ SKP Dec ⟹ Two sets of matrices $\mathbf{U}_p$, $\mathbf{V}_p$ such that:

$$\mathbf{W} = \sum_{p=1}^{P} \mathbf{U}_p \otimes \mathbf{V}_p$$

Theorem:

Let **W** be contributed by *K* SMs according to H1,H2,H3, i.e.: $\mathbf{W} = \sum_{k=1}^{K} \mathbf{C}_k \otimes \mathbf{R}_k$

then, the matrices $\mathbf{U}_k$, $\mathbf{V}_k$ are related to the matrices $\mathbf{C}_k$, $\mathbf{R}_k$ via a linear, invertible transformation defined by **exactly** $K(K-1)$ real numbers

Corollary:

If only ground and volume scattering occurs, i.e: $\mathbf{W} = \mathbf{C}_g \otimes \mathbf{R}_g + \mathbf{C}_v \otimes \mathbf{R}_v$

then, there exist two real numbers (a,b) such that:

$$\mathbf{C}_g = (a-b)^{-1}\left((1-b)\mathbf{U}_1 - b\mathbf{U}_2\right) \qquad \mathbf{R}_g = a\mathbf{V}_1 + (1-a)\mathbf{V}_2$$

$$\mathbf{C}_v = (a-b)^{-1}\left(-(1-a)\mathbf{U}_1 + a\mathbf{U}_2\right) \qquad \mathbf{R}_v = b\mathbf{V}_1 + (1-b)\mathbf{V}_2$$

Region of Physical Validity

$$\mathbf{W} \Rightarrow \boxed{\text{SKP Dec}} \Rightarrow \mathbf{U}_1, \mathbf{U}_2 \;\; \mathbf{V}_1, \mathbf{V}_2 \Rightarrow$$

$$\mathbf{C}_g = (a-b)^{-1}\left((1-b)\mathbf{U}_1 - b\mathbf{U}_2\right)$$

$$\mathbf{C}_v = (a-b)^{-1}\left(-(1-a)\mathbf{U}_1 + a\mathbf{U}_2\right)$$

$$\boxed{\text{Find } (a,b)} \Rightarrow$$

$$\mathbf{R}_g = a\mathbf{V}_1 + (1-a)\mathbf{V}_2$$

$$\mathbf{R}_v = b\mathbf{V}_1 + (1-b)\mathbf{V}_2$$

$$\mathbf{W} = \mathbf{C}_g^{True} \otimes \mathbf{R}_g^{True} + \mathbf{C}_v^{True} \otimes \mathbf{R}_v^{True}$$

W is by construction **invariant** to the choice of (a,b)

$$\mathbf{W} = \mathbf{C}_g^{True} \otimes \mathbf{R}_g^{True} + \mathbf{C}_v^{True} \otimes \mathbf{R}_v^{True} = \mathbf{C}_g \otimes \mathbf{R}_g + \mathbf{C}_v \otimes \mathbf{R}_v \quad \forall (a,b) \in \Re^2$$

How to find (a,b) ?

- Select values of (a,b) that give rise to (semi) positive definite $\mathbf{C}_g$, $\mathbf{C}_v$, $\mathbf{R}_g$, $\mathbf{R}_v$

  ⇔ Region of Physical Validity (RPV): all solutions within this region are physical validity of the solution

- Explore all the solutions within the RPV and pick the best one according to some criterion

Physically valid ground and volume coherence between passages 1 and 2

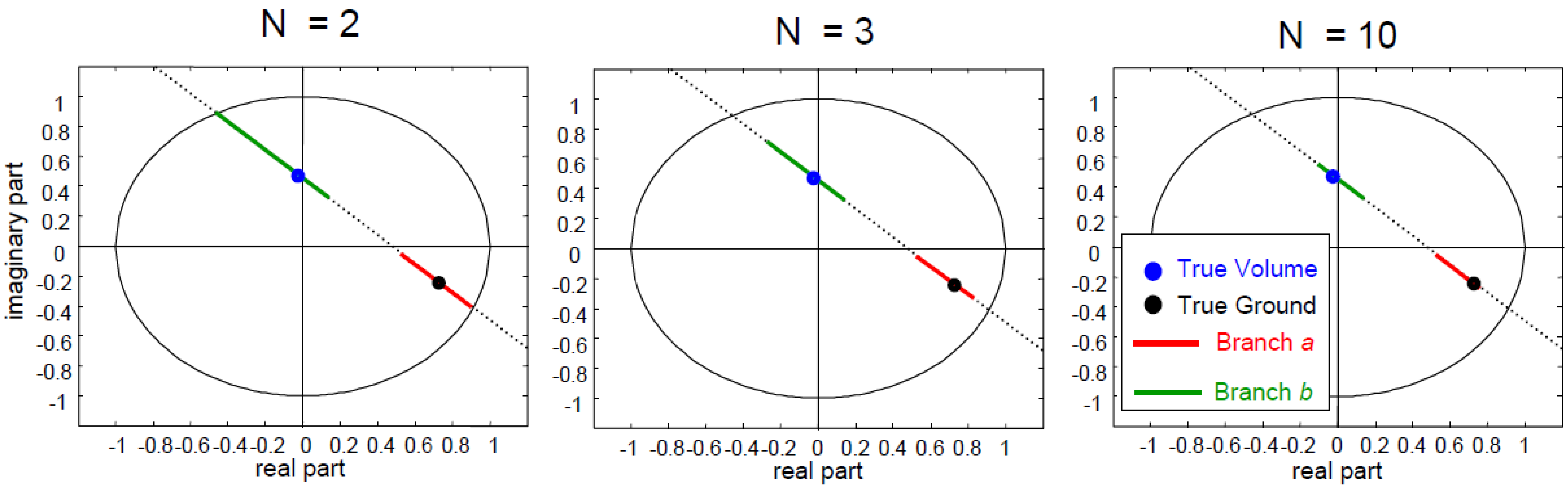

The RPV is formed by two branches, spanned by the parameters (*a*,*b*)

Single-baseline (N=2) :

The union of branches *a*, *b* results in the **same** region of physical validity as in PolInSAR

⇒ Consistency with single-baseline methods!

Multi-Baseline (N>2):

The positive definitiveness constraint results in the regions of physical validity to shrink from the outer boundaries towards the true ground and volume coherences

⇒ The higher the number of tracks, the easier it is to pick the correct solution

Boundary Solutions

By definition, the points at the outer or inner boundaries of the two branches correspond to the case where one of the four matrices $\mathbf{C}_g$, $\mathbf{C}_v$, $\mathbf{R}_g$, $\mathbf{R}_v$ is singular

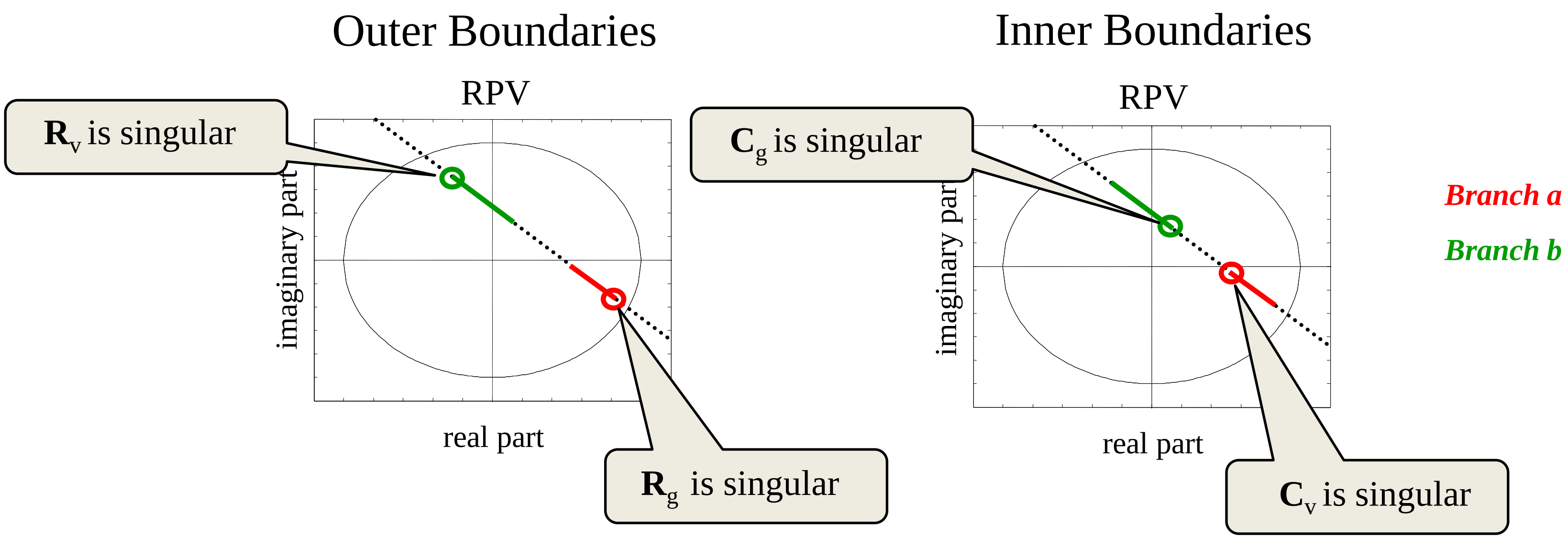

Branch *a* ⇔ **ground** structure matrix $\mathbf{R_g}$ and **volume** polarimetric signature $\mathbf{C_v}$

Branch *b* ⇔ **volume** structure matrix $\mathbf{R_v}$ and **ground** polarimetric signature $\mathbf{C_g}$

Each of the boundary solutions has a specific physical interpretation

Case Studies

Campaign	BioSAR 2007 - ESA
System	E-SAR - DLR
Period	Spring 2007
Site	Remningstorp, South Sweden
Scene	Semi-boreal forest
Topography	Flat
Tomographic tracks	9 – Fully Polarimetric
Carrier frequency	350 MHz
Slant range resolution	2 m
Azimuth resolution	1.6 m
Vertical resolution	10 m (near range) to 40 m (far range)

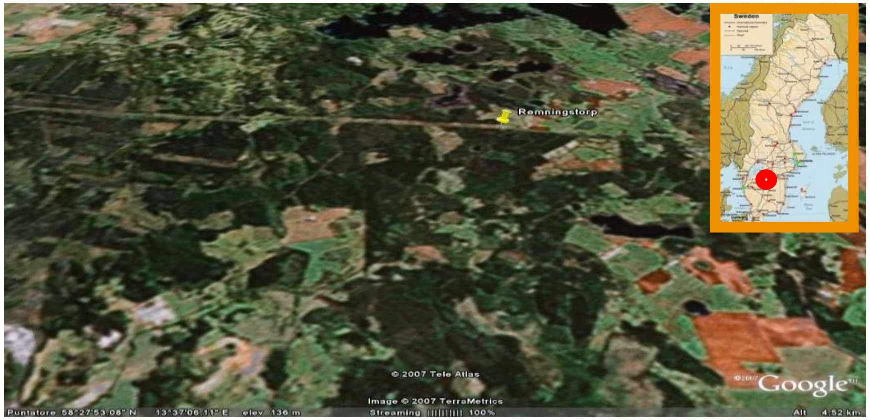

Tomographic reconstruction of an azimuth cut:

Reflectivity (HH) – Average on 9 tracks

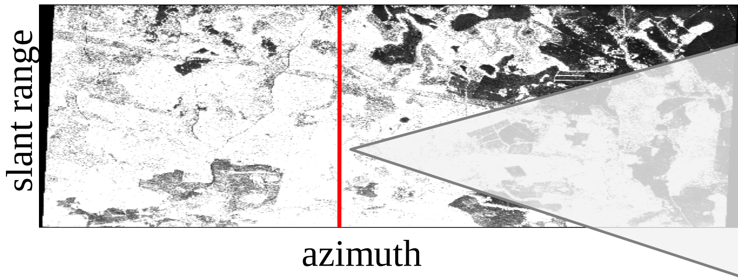

The analyzed profile is almost totally forested, except for the dark areas

HH:

- Dominant phase center is ground locked
- Vegetation is barely visible

Similar conclusions for VV

HV:

- Dominant phase center is ground locked
- Vegetation is much more visible

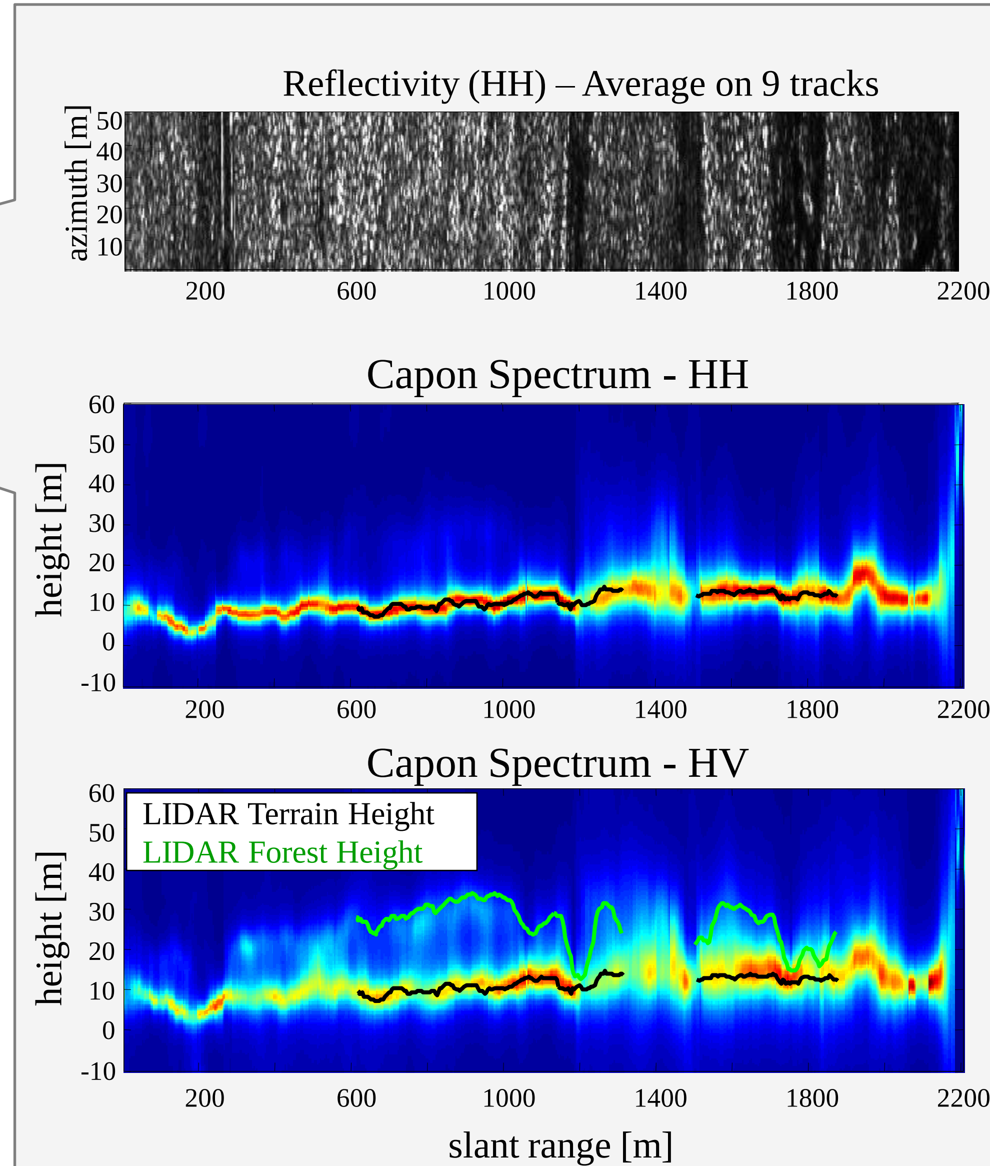

Model validation: $\mathbf{W} \overset{?}{=} \mathbf{C}_g \otimes \mathbf{R}_g + \mathbf{C}_v \otimes \mathbf{R}_v$

Methodology:

evaluation of the error between the sample covariance matrix and its best L2 approximation with $K = \{1,2,3,4\}$ KPs

$$\hat{\mathbf{W}}_K = \arg\min_{\mathbf{W}_k} \left\{ \left\| \hat{\mathbf{W}} - \mathbf{W}_K \right\|_F \right\}$$

$$error = \frac{\left\| \hat{\mathbf{W}} - \mathbf{W}_K \right\|_F}{\left\| \hat{\mathbf{W}} \right\|_F}$$

Remark: the best L2 approximation is obtained simply by taking the dominant K terms of the SKP decomposition

$$\left\| \hat{\mathbf{W}} - \hat{\mathbf{W}}_2 \right\|_F < 0.1 \cdot \left\| \hat{\mathbf{W}} \right\|_F$$

> 90 % of the information can be represented by the sum of just two KPs

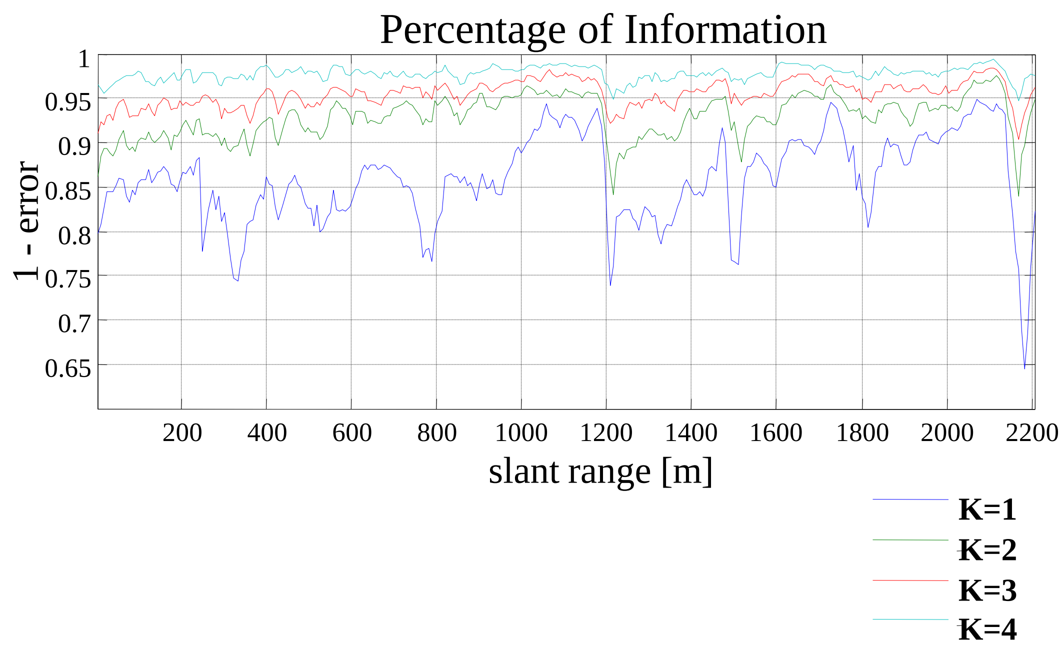

Inner boundary solutions

RPV

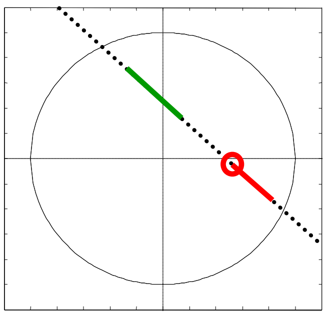

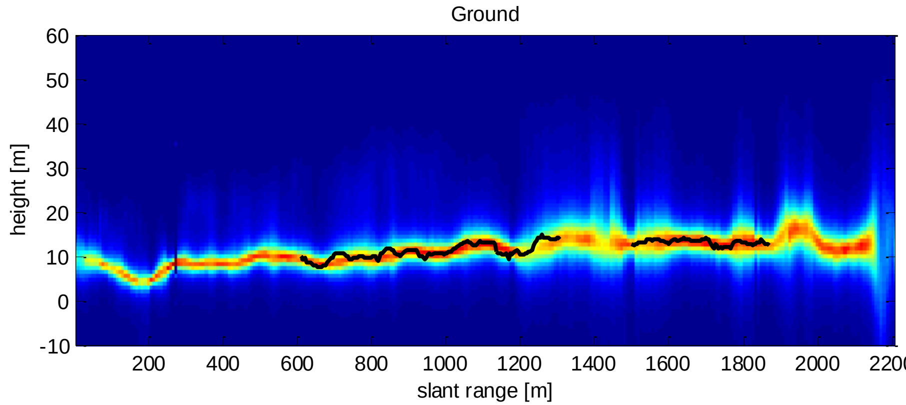

Residual volume contributions visible above the ground

Significant contributions from the ground level.
⇔ Volumetric scattering at the ground level
Consistent with:

- Backscattering from understorey or lower tree branches
- Multiple interactions of volumetric scatterers with the ground

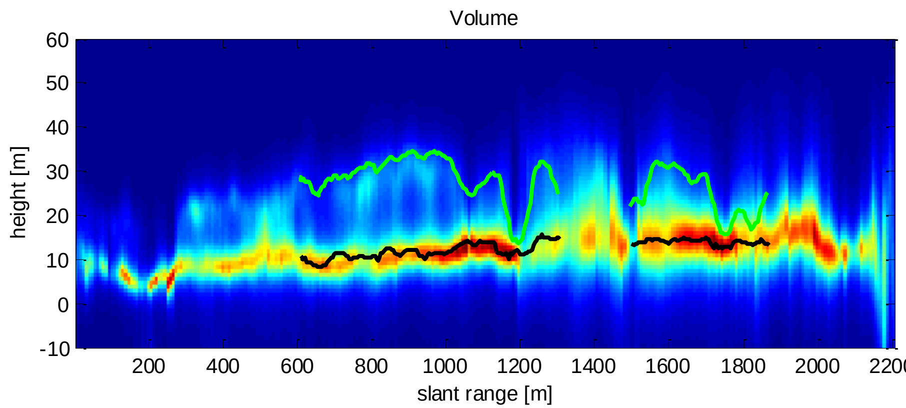

RPV

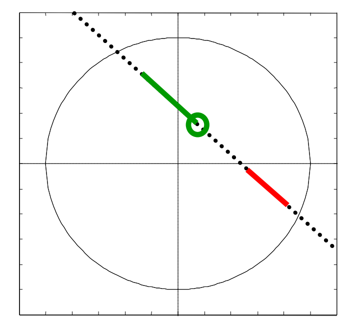

LIDAR Terrain Height
LIDAR Forest Height

Intermediate solutions

RPV

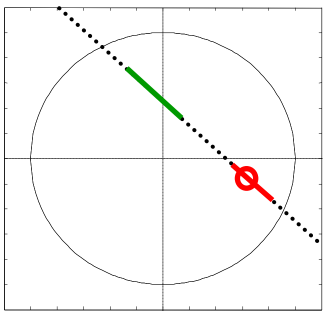

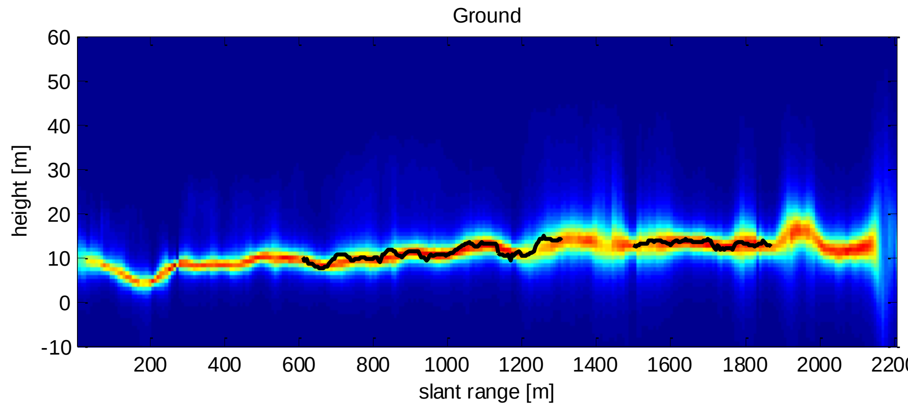

Improved volume rejection

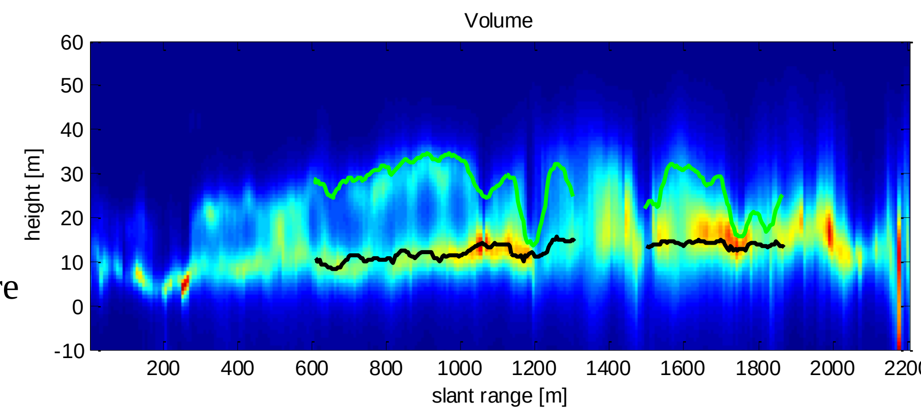

RPV

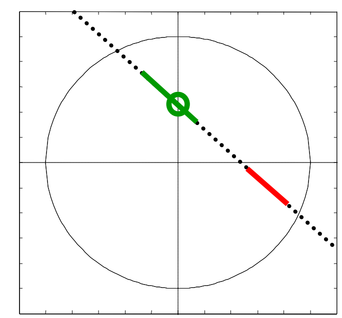

Volumetric contributions from the ground level are partly rejected

Backscattering contributions from the whole volume structure are emphasized

LIDAR Terrain Height
LIDAR Forest Height

Intermediate solutions

RPV

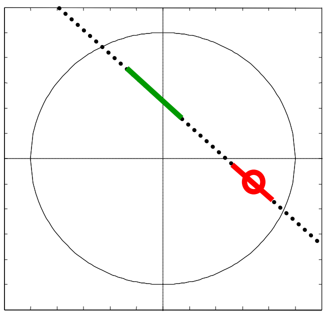

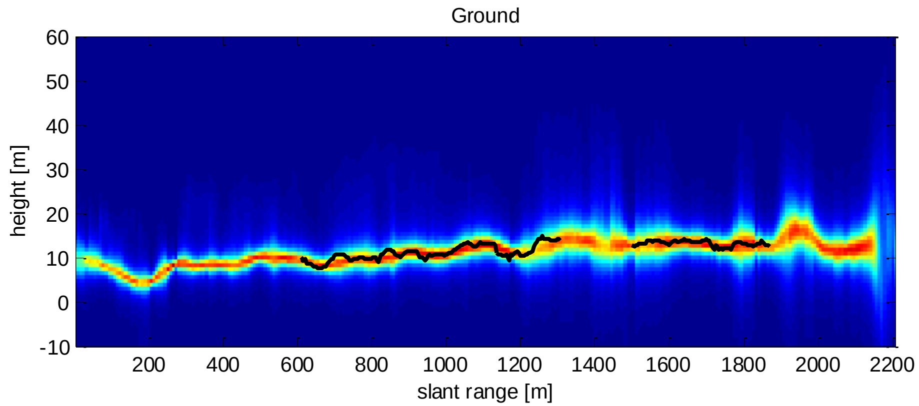

Improved volume rejection

RPV

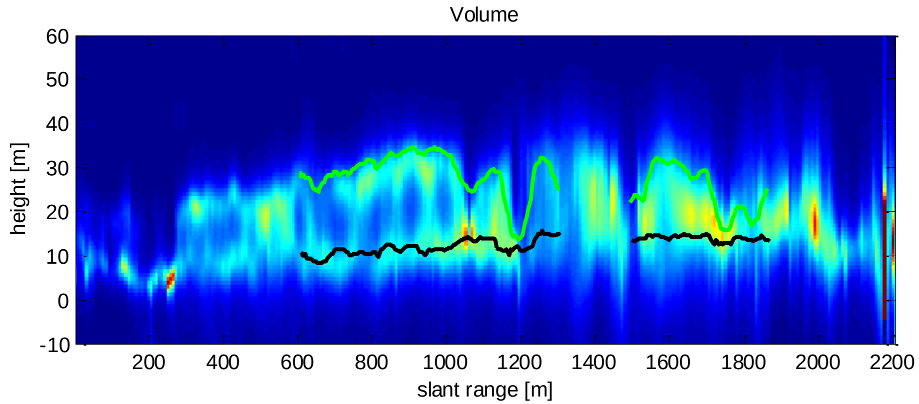

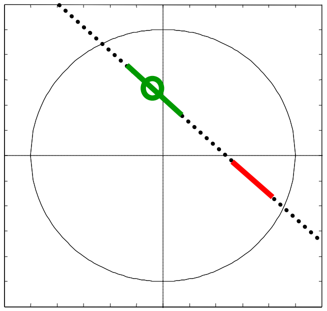

Improved ground rejection

Backscattering contributions from the whole volume structure are emphasized

LIDAR Terrain Height
LIDAR Forest Height

Intermediate solutions

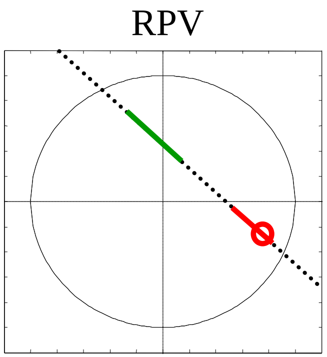

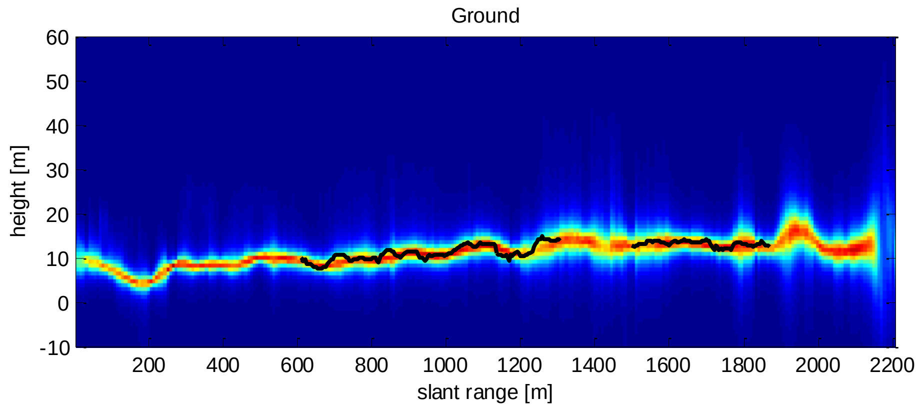

Improved volume rejection

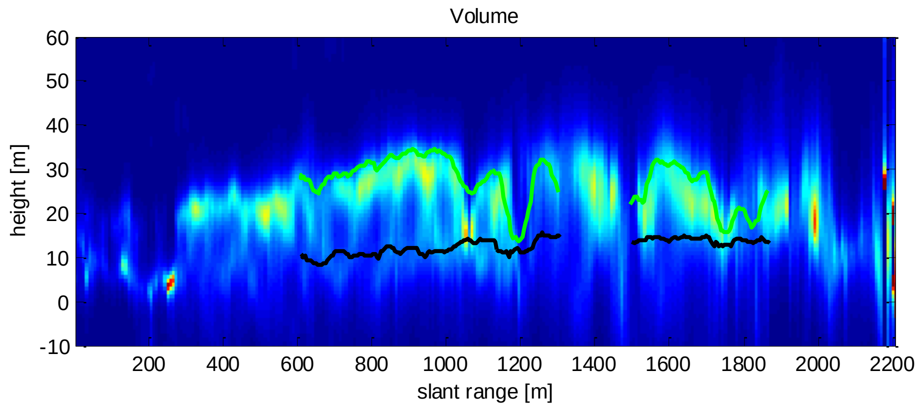

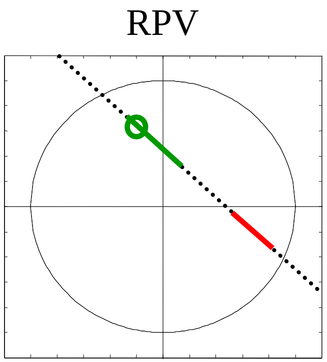

Ground contributions rejected

Contributions from the lower canopy are partly rejected

Backscattering contributions from the upper volume structure are emphasized

LIDAR Terrain Height
LIDAR Forest Height

Outer boundary solutions

RPV

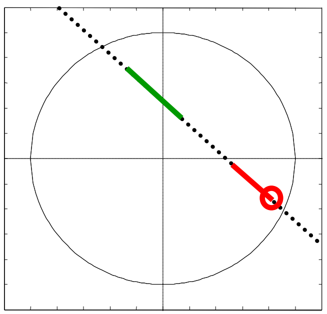

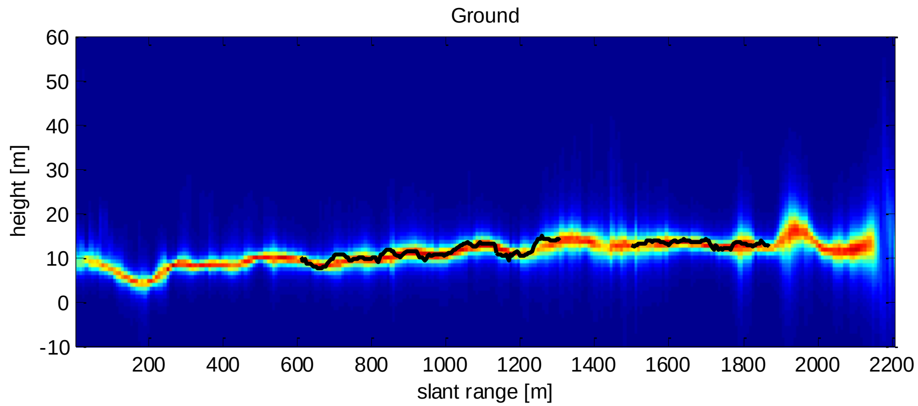

Maximum volume rejection

Ground structure is maximally coherent

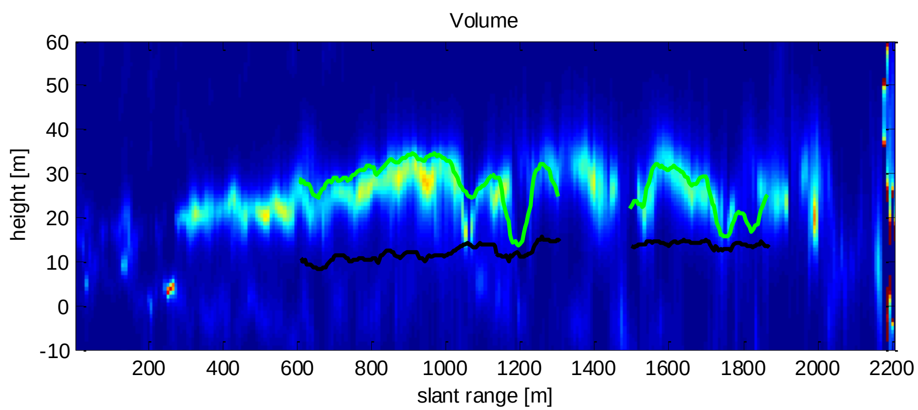

RPV

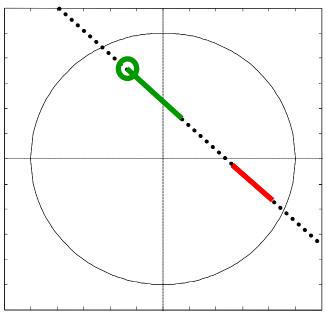

Ground and lower canopy contributions are rejected

Only upper canopy contributions are visible

Volume structure is maximally coherent

Volume top height is nearly invariant to the choice of the solution, therefore constituting a robust indicator of the volume structure

LIDAR Terrain Height
LIDAR Forest Height

Case Studies: BioSAR 2008

Campaign	BioSAR 2008 - ESA
System	E-SAR - DLR
Site	Krycklan river catchment, Northern Sweden
Scene	Boreal forest
Topography	Hilly
Tomographic Tracks	6 + 6 – Fully Polarimetric (South-West and North-East)
Carrier Frequency	P-Band and L-Band
Slant range resolution	1.5 m
Azimuth resolution	1.6 m
Vertical resolution (P-Band)	20 m (near range) to >80 m (far range)
Vertical resolution (L-Band)	6 m (near range) to 25 m (far range)

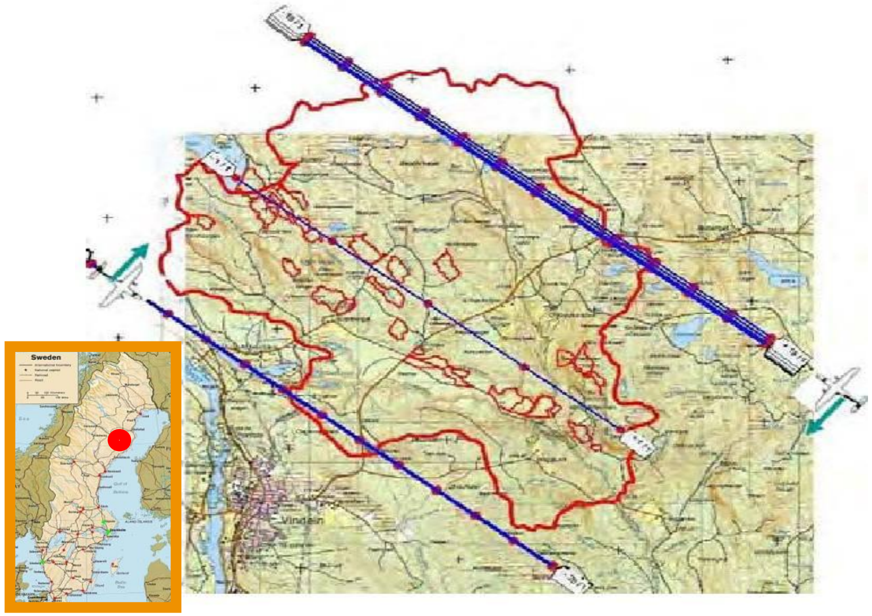

Tomographic Reconstruction of an azimuth cut:

Polarization: HV
Method: Capon Spectrum

Results are geocoded onto the same ground range, height grid

All panels have been re-interpolated such that the ground level corresponds to 0 m

Loss of resolution from near to far range, especially at P-Band ($\Delta z > 80$ m at far ranges)

Relevant contributions from the ground level below the forest are found at P-Band

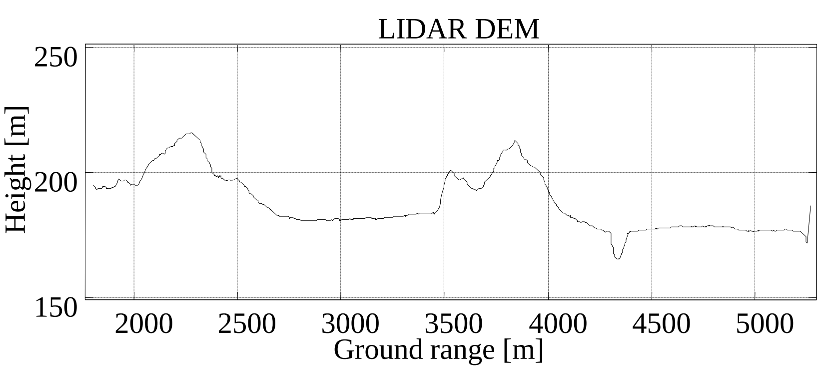

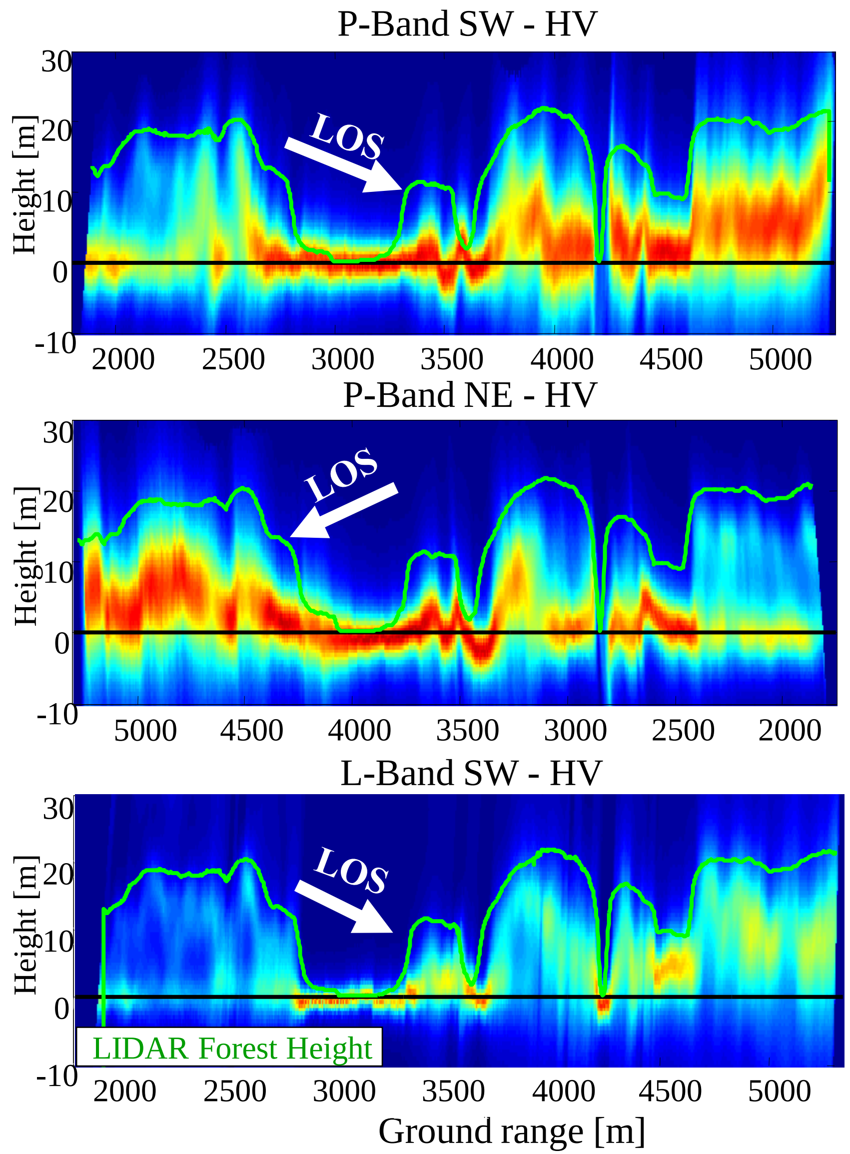

Model validation: $\mathbf{W} \overset{?}{=} \mathbf{C}_g \otimes \mathbf{R}_g + \mathbf{C}_v \otimes \mathbf{R}_v$

Methodology:

evaluation of the error between the sample covariance matrix and its best L2 approximation with *K* = {*1*,*2*,*3*,*4*} KPs

$$\hat{\mathbf{W}}_K = \arg\min_{\mathbf{W}_k} \left\{ \left\| \hat{\mathbf{W}} - \mathbf{W}_K \right\|_F \right\}$$

$$error = \frac{\left\| \hat{\mathbf{W}} - \mathbf{W}_K \right\|_F}{\left\| \hat{\mathbf{W}} \right\|_F}$$

Remark: the best L2 approximation is obtained simply by taking the dominant *K* terms of the SKP decomposition

P-Band

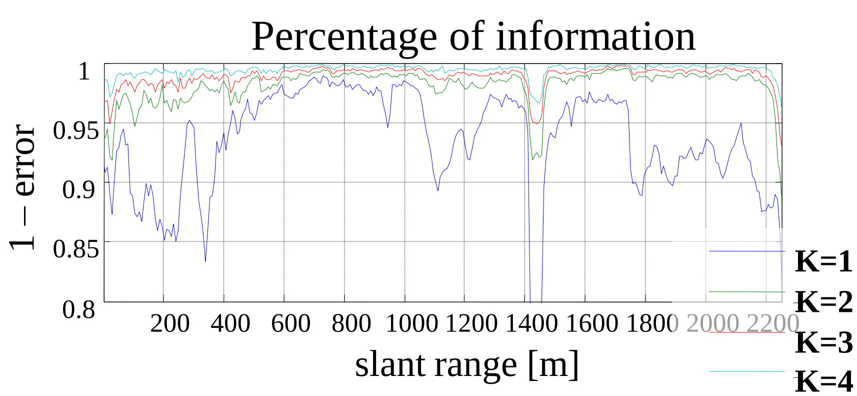

$$\left\| \hat{\mathbf{W}} - \hat{\mathbf{W}}_2 \right\|_F < 0.05 \cdot \left\| \hat{\mathbf{W}} \right\|_F$$

> 95 % of the information can be represented by the sum of just two KPs

L-Band

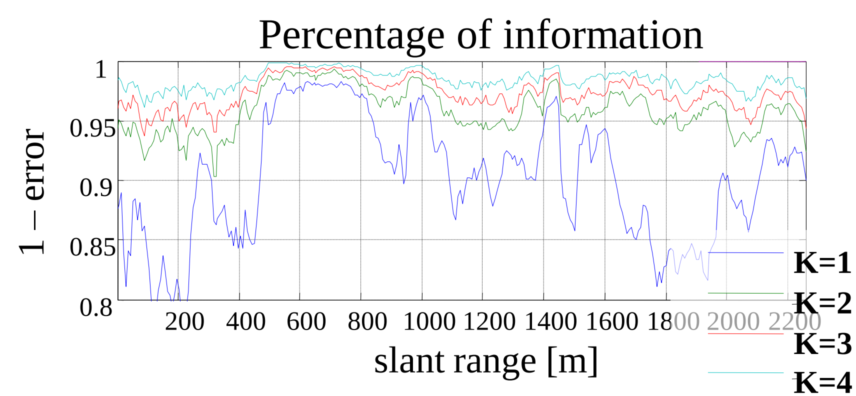

$$\left\| \hat{\mathbf{W}} - \hat{\mathbf{W}}_2 \right\|_F < 0.1 \cdot \left\| \hat{\mathbf{W}} \right\|_F$$

> 90 % of the information can be represented by the sum of just two KPs

Backscattered Power Distribution for Ground Scattering

Outer Boundary Solution

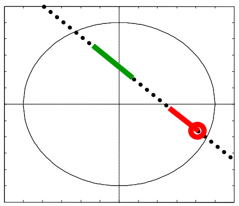

P-Band SW – Outer Boundary Solution

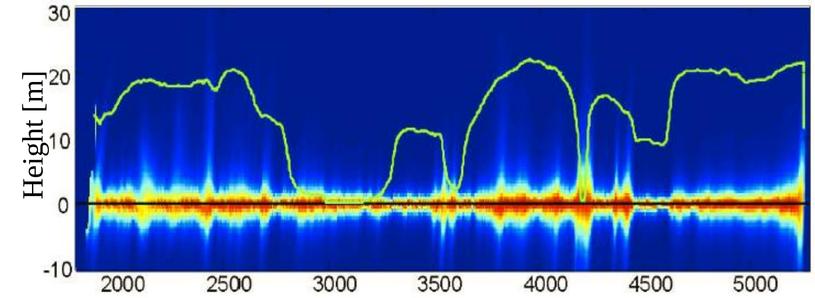

L-Band SW – Outer Boundary Solution

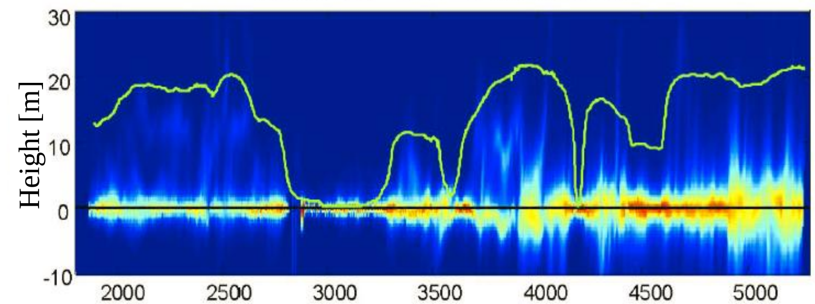

LIDAR DEM

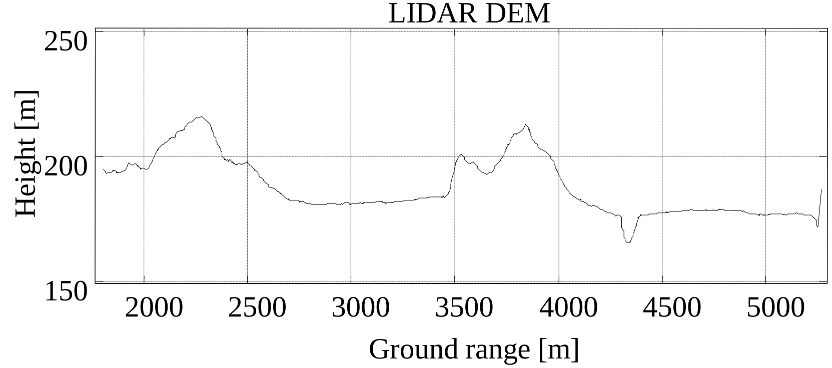

Significant rejection of volume contributions

Better results at P-Band, due to better ground visibility

Some leakage from the volume is present at L-Band in areas with dense forest and steep slopes

Backscattered Power Distribution for Volume Scattering

Inner Boundary Solution

$\mathbf{C}_g$ is singular

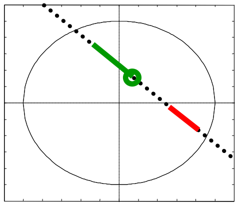

This solution corresponds to the polarization which is supposed not to be affected by ground contributions

P-Band

Significant contributions from the ground level.

⇔ Volumetric scattering at the ground level

Consistent with:

- Backscattering from understorey or lower tree branches
- Multiple interactions of volumetric scatterers with the ground

P-Band SW – Inner Boundary Solution

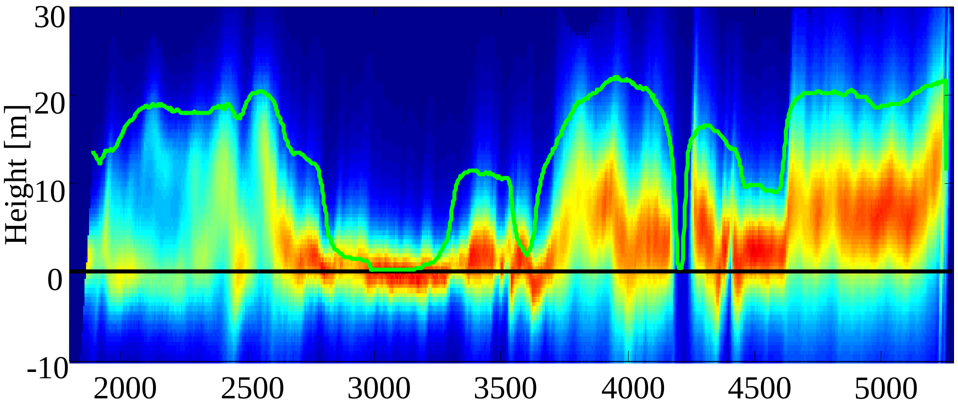

L-Band SW – Inner Boundary Solution

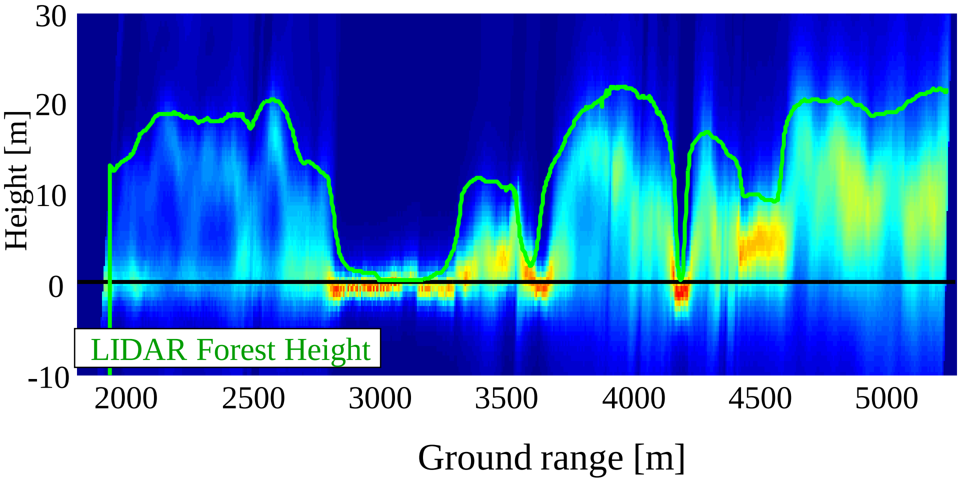

Backscattered Power Distribution for Volume Scattering

Intermediate Solution

C_g is full rank

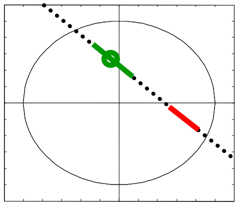

By moving from the inner to the outer boundary the contributions from the ground level are gradually rejected

P-Band
- Backscattering contributions from the whole volume structure are emphasized

L-Band
- Contributions from the lower canopy are partly rejected
- Backscattering contributions from the upper volume structure are emphasized

P-Band SW – Intermediate Solution

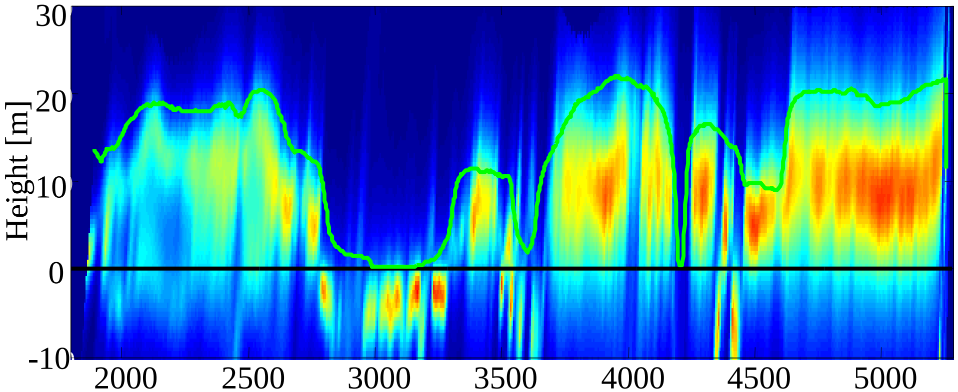

L-Band SW – Intermediate Solution

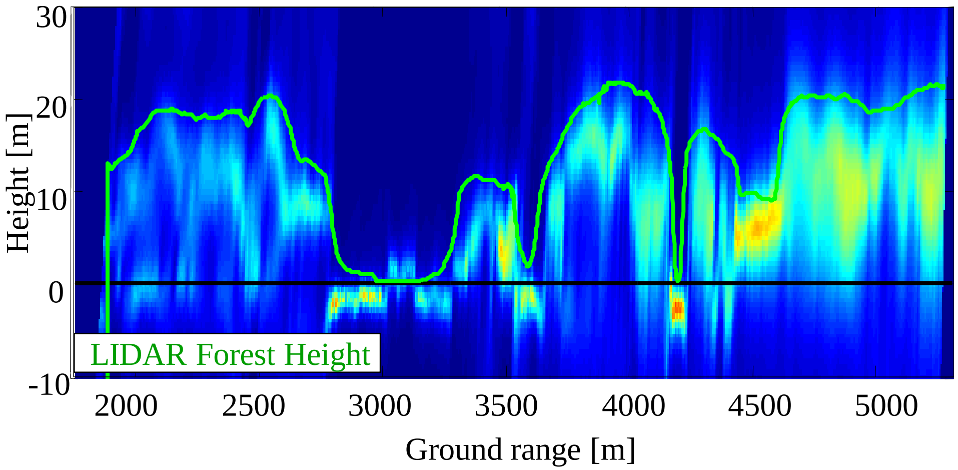

Backscattered Power Distribution for Volume Scattering

Outer Boundary Solution

C$_g$ is full rank

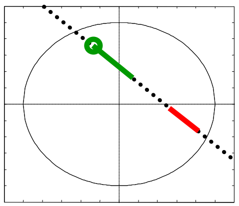

Only upper canopy contributions are visible, due to rejection of ground and lower canopy contributions

This phenomenon is more evident at P-Band, due to the coarse vertical resolution

Volume top height is nearly invariant to the choice of the solution, confirming the result of BioSAR 2007

P-Band SW – Outer Boundary Solution

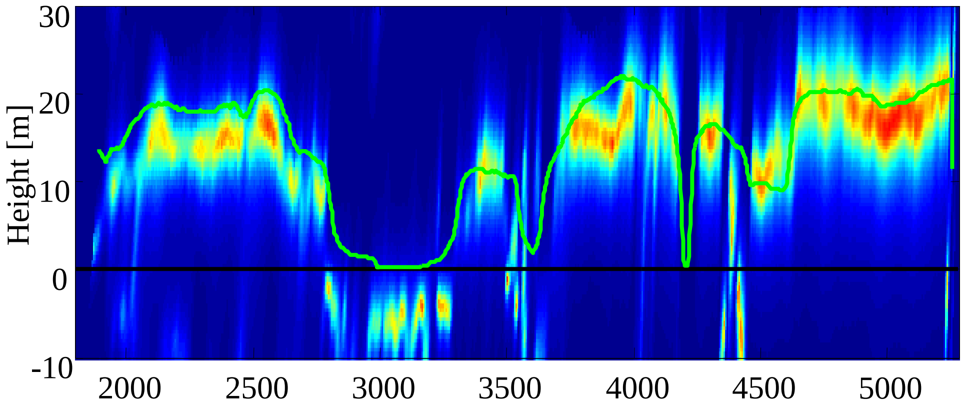

L-Band SW – Outer Boundary Solution

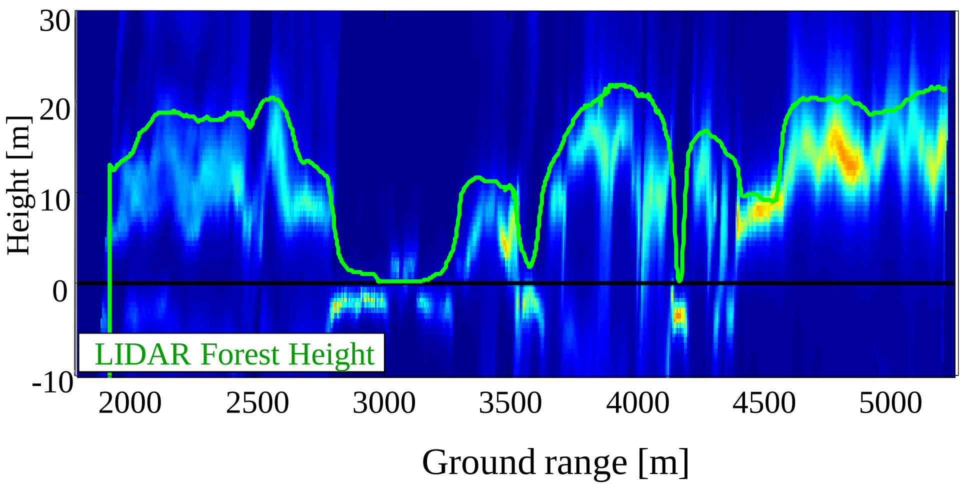

Campaign	**TropiSAR- ESA**
System	Sethi- ONERA
Period	August 2009
Site (among others)	Paracou, French Guyana
Scene	Tropical forest estimated 150 species per hectare Dominant families: Lecythidaceae, Leguminoseae, Chrysobalanaceae, Euphorbiaceae.
Tomographic tracks	6 – Fully Polarimetric
Carrier frequency	P-Band
Slant range resolution	≈1 m
Azimuth resolution	≈1 m
Vertical resolution	15 m

3D Imaging of the Guyaflux Tower

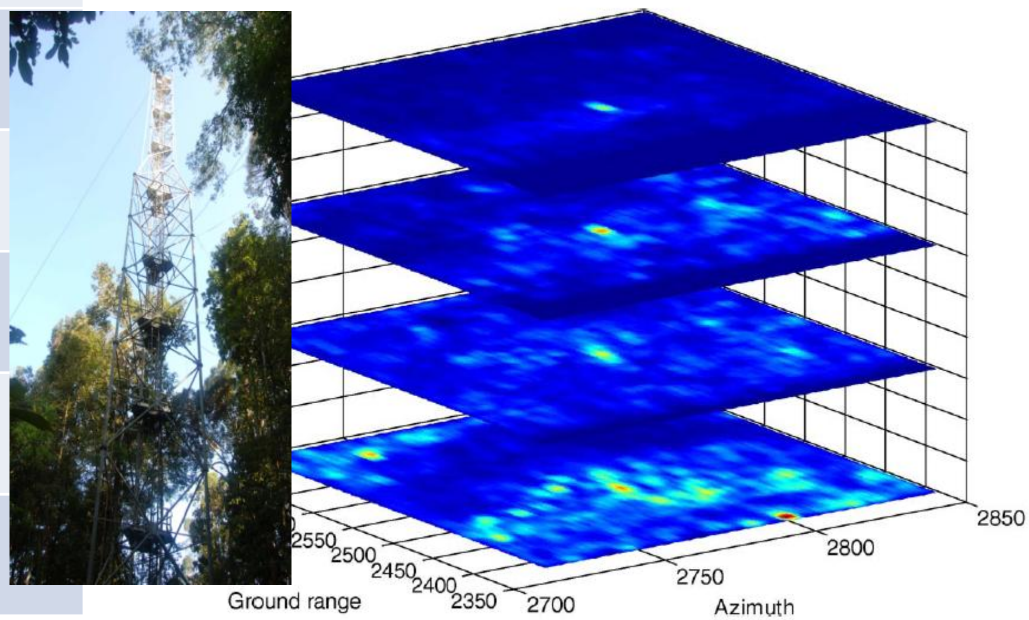

Tomographic Reconstruction of an azimuth cut:

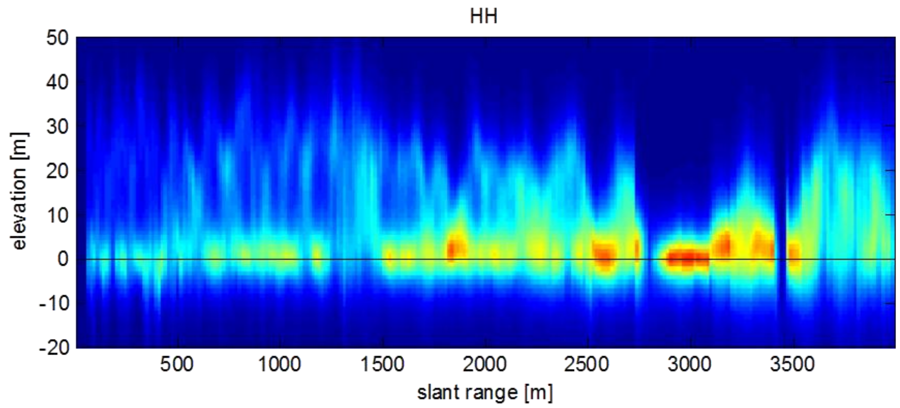

Visible contribution from the ground level beneath the forest

Vegetation is well visible

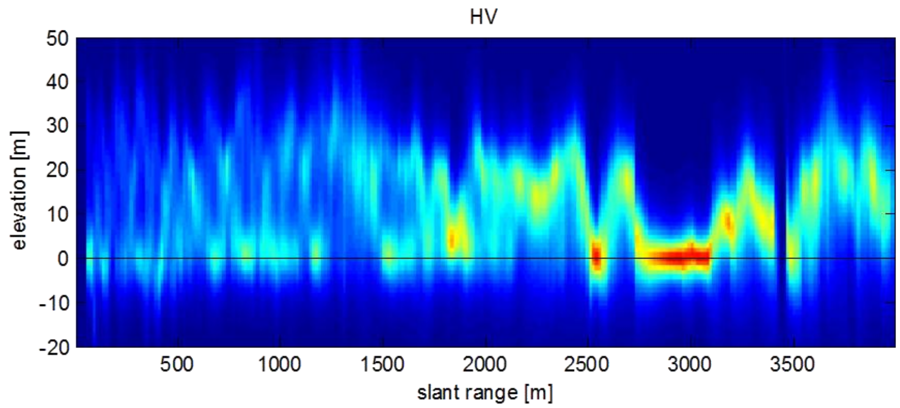

HV:
Poor contributions from the ground level beneath the forest

Vegetation is well visible

Model validation: $\mathbf{W} \overset{?}{=} \mathbf{C}_g \otimes \mathbf{R}_g + \mathbf{C}_v \otimes \mathbf{R}_v$

Methodology:

evaluation of the error between the sample covariance matrix and its best L2 approximation with $K = \{1,2,3,4\}$ KPs

$$\hat{\mathbf{W}}_K = \arg\min_{\mathbf{W}_k} \left\{ \left\| \hat{\mathbf{W}} - \mathbf{W}_K \right\|_F \right\}$$

$$error = \frac{\left\| \hat{\mathbf{W}} - \mathbf{W}_K \right\|_F}{\left\| \hat{\mathbf{W}} \right\|_F}$$

Remark: the best L2 approximation is obtained simply by taking the dominant K terms of the SKP decomposition

$$\left\| \hat{\mathbf{W}} - \hat{\mathbf{W}}_2 \right\|_F < 0.1 \cdot \left\| \hat{\mathbf{W}} \right\|_F$$

> 90 % of the information can be represented by the sum of just two KPs

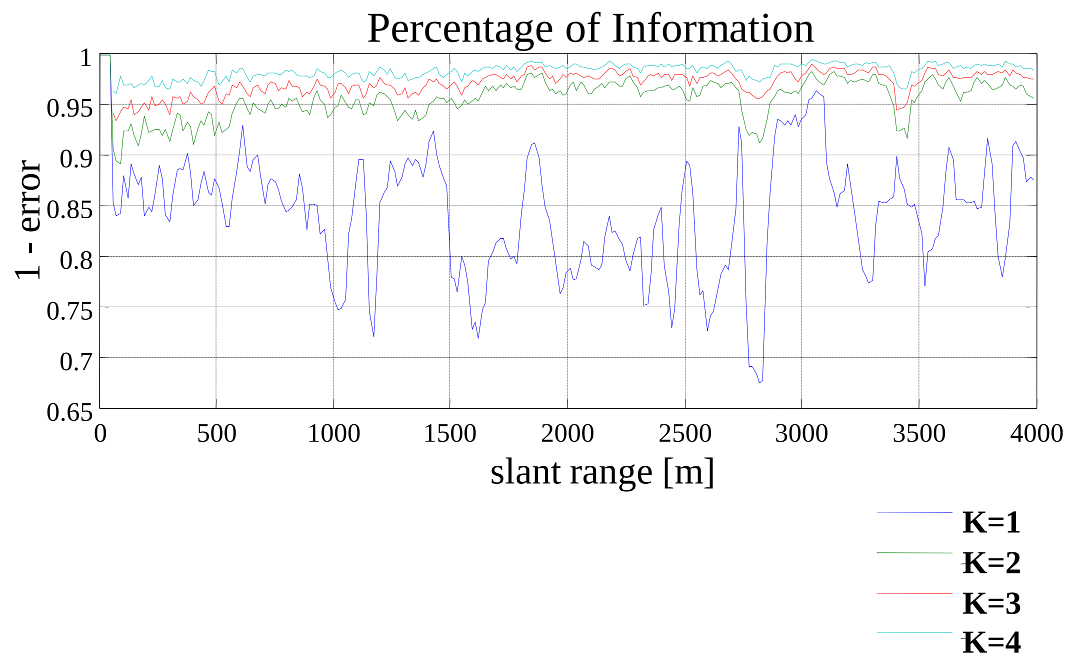

Inner boundary solutions

RPV

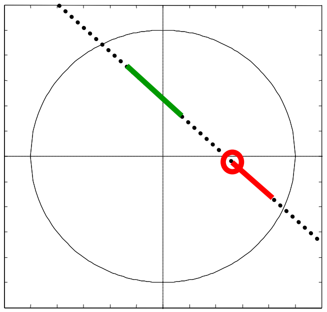

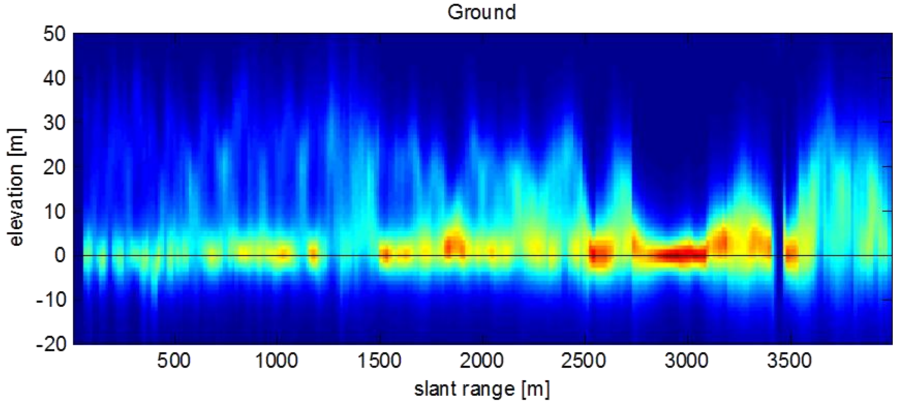

Strong volume contributions visible above the ground

Poor contributions from the ground level beneath the forest

Volume structure appears to be evenly distributed

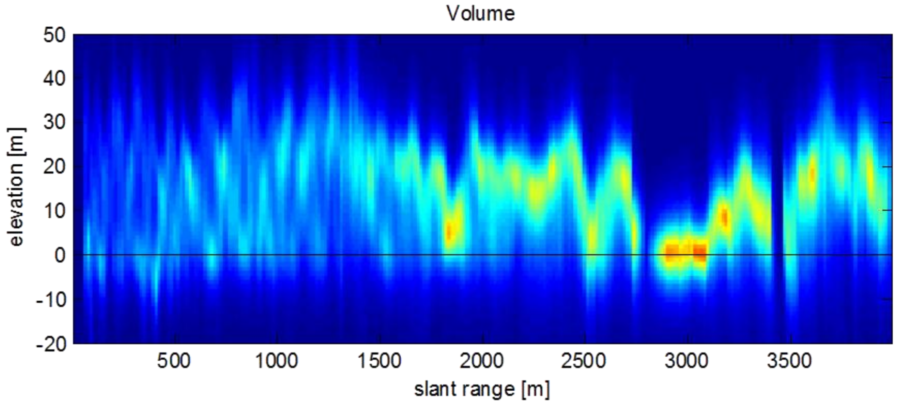

RPV

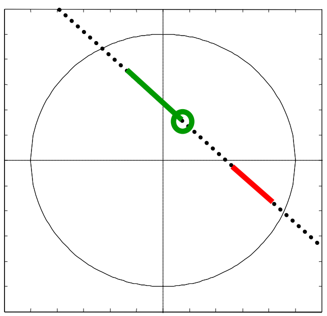

Intermediate solutions

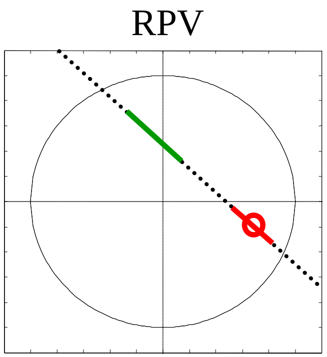

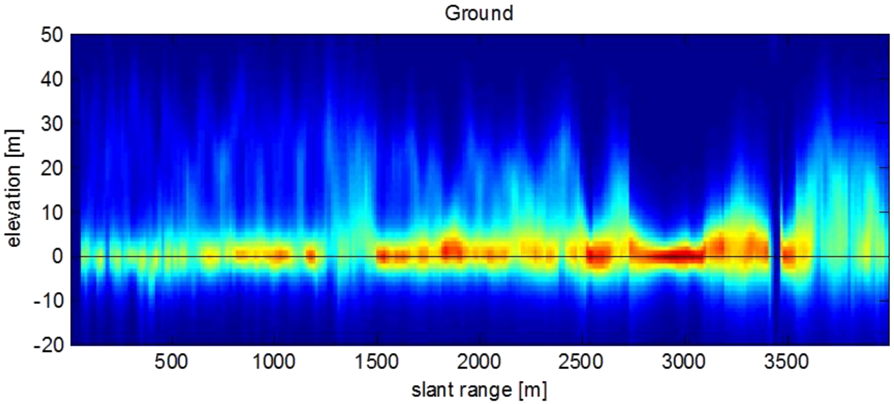

Improved volume rejection

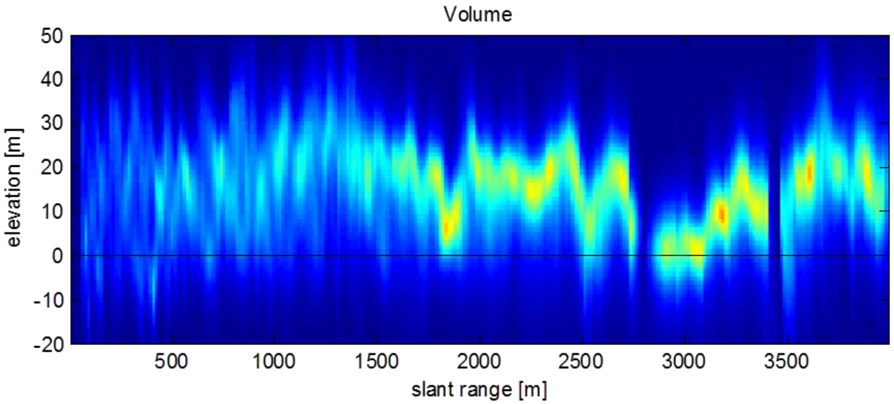

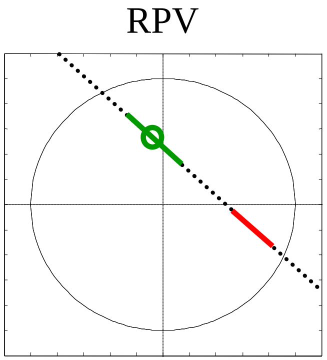

Backscattering contributions from the upper volume structure are emphasized

Outer boundary solutions

RPV

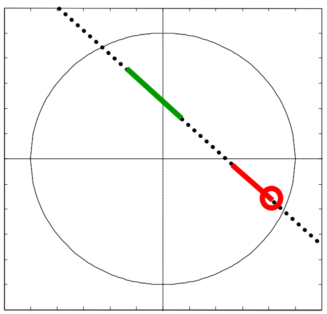

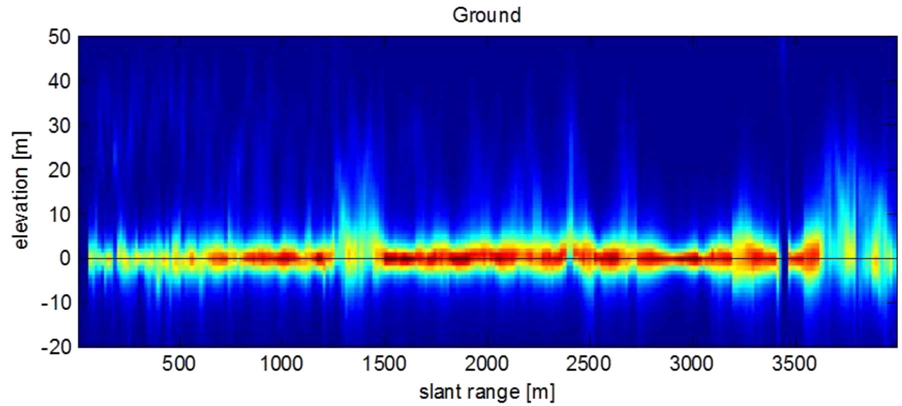

Maximum volume rejection

Ground structure is maximally coherent

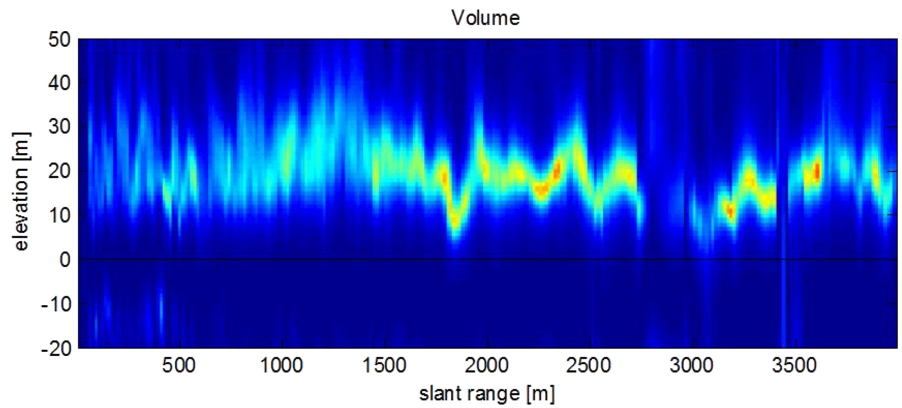

RPV

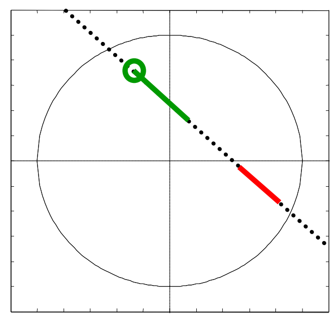

Ground and lower canopy contributions are rejected

Only upper canopy contributions are visible

Volume structure is maximally coherent

Volume top height is nearly invariant to the choice of the solution

Outline

Introduction to SAR Tomography

- Basic Concepts
- Tomographic Scene Reconstruction
- Polarimetry and Tomography: Examples
- Phase Calibration

Optimization Methods

- Multi-layer Optimization
- Multi-baseline Coherence Optimization

Ground-volume Decomposition

- Problem Statement
- SKP Structure
- SKP Decomposition
- Regions of Physical Validity
- Boundary Solutions
- Case Studies

Conclusions

MB PolInSAR

Vertical resolution ≈ 1 ÷ 15 m
N ≈ 6 ÷ 50

Vertical resolution ≈ 10 ÷ 30 m
N ≈ 6 ÷ 15

Vertical resolution >> 30 m
N ≥ 2

Single Baseline PolInSAR
N = 2

Conclusions

Multi-baseline Polarimetric SAR Tomography

○ expensive (need multiple passes)

○ non-trivial processing (accurate phase calibration, advanced Spectral Estimation techniques w.r.t. 2D SAR focusing)

Yet, it allows to ***see*** the vertical structure of distributed media (for every polarization)

⇔ Natural tool for validation and development of physical models

Joint multi-baseline – multi-polarimetric processing

○ Signal space is enlarged => further elements of diversity

⇔ Killer application for coarse vertical resolution (i.e.: few baselines) TomSAR campaigns

Where do we go now?

○ How to get radiometric accuracy ***and*** super-resolution imaging of distributed media ?

○ How to embed temporal decorrelation models into multi-baseline scenarios ?

○ 3D target reconstruction in presence of dielectric media (ice/sand).

References

Polarimetric and tomographic phenomenology of forests

- Reigber, A.; Moreira, A.; , "First demonstration of airborne SAR tomography using multibaseline L-band data," *Geoscience and Remote Sensing, IEEE Transactions on* , vol.38, no.5, pp.2142-2152, Sep 2000
- Mariotti d'Alessandro, M.; Tebaldini, S.; , "Phenomenology of P-Band Scattering From a Tropical Forest Through Three-Dimensional SAR Tomography," *Geoscience and Remote Sensing Letters, IEEE* , vol.9, no.3, pp.442-446, May 2012
- Frey, O.; Meier, E.; , "3-D Time-Domain SAR Imaging of a Forest Using Airborne Multibaseline Data at L- and P-Bands," *Geoscience and Remote Sensing, IEEE Transactions on* , vol.49, no.10, pp.3660-3664, Oct. 2011

Multi-layer optimization

- S. Sauer, L. Ferro-Famil, A. Reigber, E. Pottier, “Multi-aspect POL-InSAR 3D Urban Scene Reconstruction at L-Band”, *Eusar 2008*
- Y. Huang, L. Ferro-Famil, A. Reigber, “Under Foliage Object Imaging Using SAR Tomography and Polarimetric Spectral Estimators”, *Eusar 2010*

Coherence optimization

- M. Neumann, L. Ferro-Famil, A. Reigber, “Multibaseline Polarimetric SAR Interferometry Coherence Optimization”, *IEEE Geoscience and Remote Sensing Letters*, 2008
- E. Colin, C. Titin-Schnaider, W. Tabbara, “An Interferometric Coherence Optimization Method in Radar Polarimetry for High-Resolution Imagery”, *IEEE Transactions on Geoscience and Remote Sensing*, 2006

SKP decomposition: theory, algorithms and physical implications

- S. Tebaldini, “Algebraic Synthesis of Forest Scenarios from Multi-Baseline PolInSAR Data”, *IEEE Transactions on Geoscience and Remote Sensing*, 2009
- Tebaldini, S.; Rocca, F.; , "Multibaseline Polarimetric SAR Tomography of a Boreal Forest at P- and L-Bands," *Geoscience and Remote Sensing, IEEE Transactions on* , vol.50, no.1, pp.232-246, Jan. 2012